CHAPTER ONE

1.1 INTRODUCTION TO AVO ANALYSIS

1.1.1BACKGROUND

Seismic amplitude-versus offset (AVO) analysis has been a powerful geophysical method in aiding the direct detection of gas from seismic records. This method of seismic reflection data is widely used to infer the presence of hydrocarbons. The conventional analysis is based on such a strategy: first, one estimates the effective elastic parameters of a hydrocarbon reservoir using elastic reflection coefficient formulation; which models the reservoir as porous media and infers the porous parameters from those effective elastic parameters. Strictly speaking, this is an approximate approach to the reflection coefficient in porous media. The exact method should be based on the rigorous solutions in porous media. The main thrust of AVO analysis is to obtain subsurface rock properties using conventional surface seismic data. The Pooisson's ratio change across an interface has been of particular interest. These rock properties can then assist in determining lithology, fluid saturants, and porosity. It has been shown through solution of the Knott energy equations (or Zoeppritz equations) that the energy reflected from an elastic boundary varies with the angle of incidence of the incident wave (Muskat and Meres, 1940). This behavior was studied further by Koefoed (1955, 1962): He established in 1955 that, the change in reflection coefficient with the incident angle is dependent on the Poisson's ratio difference across an elastic boundary. Poisson's ratio is defined as the ratio of transverse strain to longitudinal strain (Sheriff, 1973), and is related to the P-wave and S-wave velocities of an elastic medium by equation 1 below. Koefoed in 1955 also proposed analyzing the shape of the reflection coefficient vs. angle of incidence curve as a method of interpreting lithology.

$$\sigma = \frac{\frac{1}{2}\left(V_p/Vs\right)^2 - 1}{\left(V_p/Vs\right)^2 - 1} \qquad \text{..... (1)}$$

In 1984, Ostrander introduced a practical application of the amplitude variation with incident angle phenomenon. He used the Zoeppritz amplitude equations (e.g. Aki and Richards, 1980) to analyze the reflection coefficients as a function of the angle of incidence for a simple three-layer, gas-sand model. The model consisted of sand layer encased in two shale layers. By using published values of Poisson's ratio for shale, brine saturated sands, and gas saturated sands, he determined that there is a significant enough change in reflection coefficient with angle of incidence to discriminate between gas saturated sands and brine saturated sands. He tested his theoretical observations with real seismic data and determined that AVO could be used as a method of detecting gas sands (Coulombe et al., 1993). AVO analysis in general, is limited by the assumptions and approximations inherent in surface seismic acquisition, processing, and interpretation. These factors include receiver arrays, near surface velocity variations, differences in geometrical spreading from near offset to far offset, dispersive phase distortion, multiples interfering with primaries, wavelet phase, source directivity and array effects (pers. Comm. R. R. Stewart, 1990). In addition, AVO analysis requires accurate determination of the angle of incidence at an interface, the accuracy of which depends on an accurate velocity model (Coulombe et al., 1993).

This method (AVO) can be explained by using this example, A 48 fold 3D seismic survey is divided into 48 constant-offset components. Each constant-offset component can be migrated (using the correct velocities) to produce a volume, giving the image of the subsurface. Each of the 48 cubes gives the same image, except that the amplitudes are different. At the same point in

all the 48 volumes the variation of the seismic amplitude with offset, h, is referred to as AVO information. The variation in amplitude can be fitted in this form of function (amp = A + $Bsin^2\theta$), where A is the intercept of AVO, B is the AVO gradient and θ is the angel of incidence. In practical world, both the estimated intercept and the gradient volumes are used in locating gas fields and other anomalies. (Rutherford et al., 1989).

The conventional treatment of seismic data, however, masks the fluid information. This problem lies with the way seismic traces are manipulated in order to enhance reflection visibility. In a seismic survey, as changes are made in the horizontal distance between source and receiver, called offset, the angle at which a seismic wave reflects at an interface also changes. Seismic traces-recordings of transmitted and reflected sound are sorted into pairs of source-receiver combinations that have different offsets but share a common reflection point midway between each source-receiver pair. This collection of traces is referred to as a common midpoint (CMP) gather. In conventional seismic processing, in which the goal is to create a seismic section for structural or stratigraphic interpretation, traces in a gather are stacked-summed to produce a single average traces. (Chiburis et al., 1993).

1.2 WHAT IS AMPLITUDE VERSUS OFFSET/ANGLE (AVO/AVA)

In geophysics, amplitude versus offset (AVO) or amplitude variation with offset is a variation in seismic reflection amplitude with change in distance between shot point and receiver that indicates differences in lithology and fluid content in rocks above and below the reflector. It is also referred as AVA (amplitude variation with angle). As AVO studies are being done on CMP data, the offset increases with the angle (Schlumberger Oilfield Glossary).

An AVO anomaly is most commonly expressed as increasing (rising) AVO in a sedimentary section, often where the hydrocarbon reservoir is "softer" (lower acoustic impedance) than the surrounding shale. Typically amplitude decreases (falls) with offset due to geometrical spreading, attenuation and other factors. An AVO anomaly can also include examples where amplitude with offset falls at a lower rate than the surrounding reflective events (Schlumberger Oilfield Glossary). In theory, as the AVO phenomena translates the sharing of the energy of the incident compressible wave between the compressible and converted reflections, the observation of the converted mode AVO would be redundant. In some privileged areas, the AVO of compressible waves effectively provides the expected information. In most cases, single fold data are not pure enough to provide reliable amplitude measurements, and finally the result will be doubtful (Xu, Y and Bancroft, J. C., 1997)

1.2.1 SEISMIC ENERGY PORTIONING AT BOUNDARIES

Amplitude variation with offset comes about from something called ‘energy partitioning’. When seismic waves hit a boundary, part of the energy is reflected while part is transmitted. If the angle of incidence is not zero, P wave energy is partitioned further into reflected and transmitted P and S components. The amplitudes of the reflected and transmitted energy depend on the contrast in physical properties across the boundary. For seismic people, the important physical properties in question are compressional wave velocity (Vp), shear velocity (Vs) and density (ρ). But, the important thing to note is that reflection amplitudes also depend on the angle-of-incidence of the original ray as shown in the figure 1

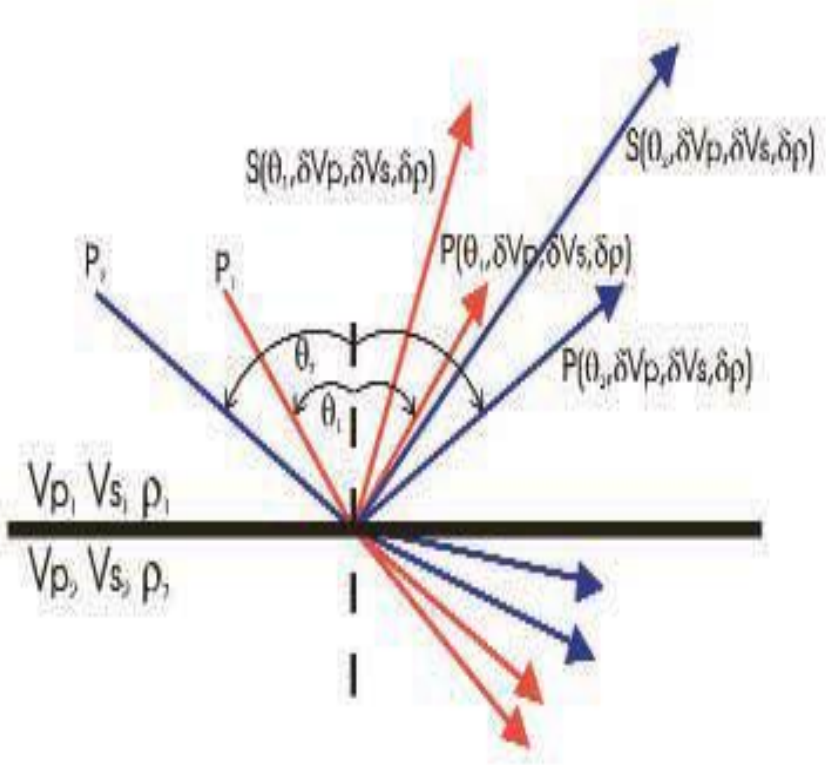

Fig 1: A seismic wavefront hitting a reflector. The physical properties are different on either side of the reflector.

How amplitudes change with angle-of-incidence for elastic materials is described by the quite complicated 'Zoeppritz equation (as well as higher-level approximations like that of Aki and Richards in their famous seismology textbook of 1979). But there are many different simplications of these equations that make analysis of amplitudes with angle much easier. One thing to point out now is that 'amplitude variation with offset' is not always an appropriate term. For proper analysis, we need 'amplitude variation with angle'.

The Zoeppritz equations describe the reflections of incident, reflected, and transmitted P waves and S waves on both sides of an interface. For analysis of wave reflection we need an equation

which relates reflected wave amplitudes to incident wave amplitudes as a function of angles of incidence. In the past decade, many forms of simplifications of Zoeppritz equation of P-P reflection coefficient appeared in the literature and industrial practice (Aki and Richards, 1980, Shuey, 1985, Parson, 1986, Smith and Gidlow, 1989, Verm and Hilterman, 1994). Each of these simplifications in a degree links reflection amplitude with variations of rock properties. Aki and Richards (1980) give the approximation of P-S reflection coefficient. There is also a rough approximation linking P-S reflection coefficient with pure SH reflection coefficient (Fraiser and Winterstein, 1993, Stewart, 1995). Because of the challenges in the processing of the real radial data which are mainly P-S reflections, applications of P-S reflection coefficient and AVO analysis rarely appear in the literatures and practice (Xu, Y and Bancroft, J. C., 1997).

1.2.2 MECHANICS OF QUANTITATIVE AVO ANALYSIS.

Quantitative AVO analysis is done on common-midpoint-gathers (or super-gathers, or common-offset gathers, or as they are called in the AVO business 'Ostrander gathers' (Ostrander 1984). At each time sample amplitude values from every offset in the gather are curve-fit to a simplified, linear AVO relationship as in Figure 2. A better way of saying this is that we fit a best-fit straight line to a plot of amplitude versus some function of the angle of incidence. This yields two AVO attributes-basically the slope and intercept of a straight line, which describes, in simpler terms how the amplitude behaves with angle of incidence. There are a lot of equations that have been used over the last 15 years or so, but all of them, no matter what interpretation is given to the 'intercept' and 'slope', work in this same way.

1.3 THEORY OF AVO/AVA

Basic AVO theory is well understood because it is widely used as a tool in hydrocarbon detection (Smith, 1987). A few of the most important ideas will be highlighted to keep in mind when doing AVA analysis. Figure 1 above shows the theoretical energy partition at an interface. This figure illustrates an important point that accounts for AVA phenomena: the conversion of P-wave energy to S-wave energy. Though the majority of seismic data is recorded simply as a single component pressure wave, the fact that the Earth is elastic causes amplitudes of P-wave arrivals to be a function of S-wave reflection coefficient (Rs) (Castagna, J. P., and Smith, S.W., 1994). In practice, Rs is tricky to obtain and the P-wave reflection coefficient (R_p) is what we have in the vast majority of cases (Smith, G.C., and Sutherland, R.A., 1996).

Several attempts at the practical application of AVO began about 15years ago, but the physics draws on 19^{th} century advances in optics and electromagnetic wave theory. Green and Kelvin made some speculation about the similarity of the reflective behavior of light and elastic waves in the 1800s (Green 1871). Using Snell's law, Knott in 1899, and Zoeppritz in 1919, developed general expressions for the reflection of compressional and shear waves at a boundary as a function of the densities and velocities of the layers in contact (Knott 1899 and Zoeppritz 1919). Although Zoeppritz was not the first to publish a solution, his name is associated with the cumbersome set of formulas describing the reflection and refraction of seismic waves at an interface. In 1936, Macelwane and Sohon recast the equations to gain insight into the physics and facilitate calculations (Macelwane et al 1936). Before the advent of computers, AVO effects

were incorporated into synthetic seismograms and other calculations using approximated Zoeppritz equations (Muskat et al 1940, Koefod 1955 and Bortfeld 1961). Today, personal computers can generate synthetics based on the full Zoeppritz formalism, but approximations are still used to gain physical insight into the relative influence of velocity and density changes on seismic amplitudes, and in the attempt to back out lithology and fluid type from AVO data (Aki et al 1980).

1.4 APPLICATION OF AVO/AVA

AVO has its most common application in hydrocarbon reservoirs , i.e. it is used by geophysicists to determine thickness, porosity, density, velocity, lithology and fluid content of rocks. For successful AVO analysis, special processing of seismic data and seismic modeling is needed to determine rock properties with a known fluid content. This knowledge makes it possible to model other types of fluid content. A gas-filled sandstone might show increasing amplitude with offset, whereas a coal might show decreasing amplitude with offset. AVO rising is typically seen in oil-bearing sediments, and even more so in gas-bearing sediments. Particularly important examples can be observed in turbidite sands such as the Late Tertiary deltaic sediments in the Gulf of Mexico (especially during the 1980s-1990s), West Africa, and other major deltas around the world. AVO is most routinely used by most major companies as a tool to "de-risk" exploration targets and to better define the extent and the composition of existing hydrocarbon reservoirs.

In AVO analysis, practices mainly focus on looking for more sensitive indicator of hydrocarbon and extracting and exploiting anomalous variations between seismic and these

sensitive parameters. Some authors (Goodway et al., 1997) showed the advantages of converting velocity measurements to Lame's moduli parameters (λ and μ) to improve identification indicator of reservoir zones. Castagna et al (1985) observed a few relationships of compressible wave and shear wave in the elastic silicate rocks. These give us good empirical guidance to study the rock property from seismic data.

Least square regression analysis an inversion is the common approaches in the AVO analysis. In 1986, Parson obtained contrasts of three elastic parameters (λ, μ and ρ) by pre-stack inversion. Goodway et al (1997) obtained the Vp and Vs from inversion and converted them to the λ/μ to detect the reservoirs. However, the non uniqueness is always the problem in the seismic inversion. The background velocity error causes the ratio to change greatly or eliminates the high frequency contrast. Appropriate selection of parameters, background velocity, wavelet estimation, application of a priori information is still important issues which remain to be resolved. The least square regression analysis is used to extract elastic parameters from pre-stack data. The extraction provides band-limited information on which attempt to discover anomaly caused by hydrocarbon reservoirs (Xu, Y and Bancroft, J. C., 1997).

An important caveat of AVO analysis using only P-energy is its failure to yield a unique solution, so AVO results are prone to misinterpretation. One common misinterpretation is the failure to distinguish a gas-filled reservoir from a reservoir having only partial gas saturation ("fizz water"). However, AVO analysis using source-generated or mode-converted shear wave energy allows differentiation of degrees of gas saturation. Not all oil and gas fields are

associated with an obvious AVO anomaly (e.g. most of the oil found in the Gulf of Mexico in the last decade), and AVO analysis is by no means a panacea for gas and oil exploration.

1.5 PROBLEM STATEMENT

In the late 1920s, the seismic reflection technique became a key tool for the oil industry, revealing shapes of subsurface structures and indicating drilling targets. This has developed into a multibillion dollar business that is still primarily concerned with structural interpretation. But advances in data acquisition, processing and interpretation now make it possible to use seismic traces to reveal more than just reflector shape and position. Changes in the character of seismic pulses returning from a reflector can be interpreted to ascertain the depositional history of a basin, the rock type in a layer, and even the nature of the pore fluid. This last refinement, pore fluid identification, is the ultimate goal of AVO analysis. Amplitude variation with offset, AVO, has become an essential tool in the petroleum industry for hydrocarbon detection (Rutherford and Williams, 1989). AVO responses vary depending on the physical parameters of the reflection interface and incidence angle (Shuey, 1985). In relatively simple geologic settings, offset is a simple function of angle (Castagna and Smith, 1994). However, a more realistic V (z, m) will make offset and incidence angle a complex relation (Sheriff, 1995). In these settings, amplitude variation with angle (AVA) is a preferable alternative to AVO analysis. Among the various seismic technique for hydrocarbon detection and monitoring in the subsurface, Amplitude variation with offset (AVO) methods appear to be quite promising. The AVO is measured in the primary P-wave

reflections, which are the strongest and freest from contamination, and at the same time, they contain the information about the S-wave reflectivity. Many theoretical models were established based on AVO equations in fluid-gas media; however, still little research has been done on time-lapse AVO attributes in real data. It is therefore necessary to perform further research on the use of AVO analysis on seismic data.

1.6 JUSTIFICATION OF THE THESIS.

Early practical evidence that fluids could be seen by seismic waves came from "bright spots"-streaks of unexpectedly high amplitude on seismic sections, often found to signify gas. Bright spots were recognized in the early 1970s as potential hydrocarbon indicators, but .drillers soon learned that hydrocarbons are not the only generators of bright spots. High amplitudes from tight or hard rocks look the same as high amplitudes from hydrocarbons, once seismic traces have been processed conventionally. Only AVO analysis, which requires special handling of the data, can distinguish lithology changes from fluid changes. (Chiburis et al., 1993).

It has been two decades, for the quick development in seismic exploration. AVO technology has remarkably advanced and has been extensively implemented in oil industry. Nevertheless, the Zoeppritz equation considers only the elastic properties of the rocks ignoring the non elastic properties such as velocity dispersion attenuation. Considering all these things, there are still problems that the traditional AVO technology is not able to handle adequately.Over the period of time, Geophysicists have noticed low-frequency seismic anomalies associated with hydrocarbon reservoirs and this topic is gained more and more attention.

The great promise of amplitude-versus-offset (AVO) analysis lies in the dependence of the offset-dependent-reflectivity of reflected compressional waves on the elastic properties of the subsurface. As different lithologies may exhibit distinct Poisson's ratios and gas bearing strata usually exhibit anomalously low Poisson's ratios. AVO has been recognized as a potential seismic lithology tool and direct hydrocarbon indicator. Unfortunately, experience has shown that the theoretical potential for AVO analysis is, all too often, not realized in practice. Despite some notable successes, it cannot be claimed that economic impact of AVO analysis is on a par with other breakthrough in geophysical technology such as a bright spot analysis or 3D seismic surveys. This lack of penetration of AVO into the mainstream as an interpretation technology is not due to any inherent lack of validity of the concept, but rather due to a lack of credibility of the concept in the minds of potential practitioners (Castagna, 1995).

The purpose of this thesis is to consider the basics of amplitude variations with offset (AVO). It will also be demonstrating the idea that changes in seismic amplitude with offset (AVO effects) are due to contrasts in the physical properties of rocks. Moreover, further, quantitative analysis of AVO effects can yield attributes that discriminate between lithologies and fluids. Further analysis can also lead directly to estimates of the elastic properties that will give rise to the AVO effects and also reduce the uncertainties of interpretation.

1.7 RESEARCH OBJECTIVES

1. The basic goal in this study is to obtain subsurface rock properties using conventional surface seismic data.
2. To use AVO to interpret data as an aid to identify the types of layers in a reservoir.

3. To use AVO analysis to predict the characteristics of a reservoir and to make a preliminary determination of the type of material and its detectability of its AVO response.
4. To look at the physical cause of AVO behavior.
5. An AVO effect is used to estimate the elastic properties of the reservoir.

CHAPTER 2

LITERATURE REVIEW

2.1 INTRODUCTION

Considering the conventional utilization of the seismic reflection method, it has been assumed traditionally that seismic signals can be viewed as a band-limited normal incidence reflection coefficient series with appropriate travel time and amplitude variation due to propagation through an overload. It has been demonstrated that gas sand reflection coefficient vary in anomalous fashion with increasing offset, it also displayed how to utilize this anomalous behavior as a direct indicator of hydrocarbons in relation to real data (Ostrander, 1982). This work done by Ostrander made the methodology commonly known as amplitude variation with offset analysis (AVO) very popular. Moreover, this method is not only "Seismic lithology" but it also provides an enhanced model of the reflection seismogram which allows one to better estimate both "background velocities" and normal incidence reflection (Castagna, 1993).

Exploration geophysics can be considered as a science of anomalies to a considerable extent. Most of the hydrocarbons discovered about fifty years ago can safely be assumed to be associated with some kind of geophysical anomaly. Explorationists routinely make use of deviations from expected gravity, seismic travel time and seismic amplitude without recovering uniquely determined absolute density, depth or reflectivity. Consequently, significant risk is associated with drilling a well, even when all the technology and analysis available have been thrown at the problem. Experience has shown that geophysical anomalies can be used to reduce risk, and consequently, to identify new prospects (Castagna, 1993).

Thus, one would expect the exploration geophysicist, who is concerned primarily with finding hydrocarbons, to have somewhat different expectations from AVO analysis, than say a research physicist, who may be primarily concerned with getting the right answer. Taking the latter approach, if one makes very simplistic assumptions, methods can be developed which work well on synthetic data. However, the more one appreciates the complexities of the real world with real geology, the more it becomes apparent that AVO analysis does not work. The only negative side of this conclusion is that, people are successfully still using AVO anomalies to find hydrocarbons throughout the world. The geophysicist does not require answers that are absolutely correct, acceptable range of deviations from some background trend may be sufficient for instance the magnitude of the deviation in absolute units may not even be required. A very vivid analogy is the spontaneous potential (SP) log. If one is told that an SP log reading is -30 millivolts at some depth, the rock properties cannot be interpreted from this even with the most complex modeling and inversion schemes. This is because the SP log is an anomaly log with no meaningful absolute scale. When it is noted that 30 millivolts is quite a phenomenal deviation from the background trend which is produced by surrounding shale, It can be said that the SP log is very important in identifying sands (Castagna, 1993).

2.2 PRINCIPLES OF AVO/AVA.

In exploration geophysics, simple isolated interfaces are scarcely dealt with. However, our understanding of offset-dependent reflectivity must begin with portioning of energy at just such interface (Castagna and Backus, 1993). In the Figure below, the angles of incident, reflected and transmitted rays synchronous at the boundary are related according to snell's law by:

$$p = \frac{\sin\theta_1}{V_{p1}} = \frac{\sin\theta_2}{V_{p2}} = \frac{\sin\phi_1}{V_{s1}} = \frac{\sin\phi_2}{V_{s2}} \quad \text{..... (2)}$$

Where V_{p1} = P-wave velocity in medium 1, V_{p2} = P-wave velocity in medium 2; V_{s1} = S-wave velocity in medium 1; V_{s2} = S-wave velocity in medium 2; θ_1 = incident P-wave angle, θ_2 = reflected S-wave angle, ϕ_1 = reflected S-wave angle, ϕ_2 = transmitted S-wave angle, and p is the ray parameter (Castagna et al, 1993).

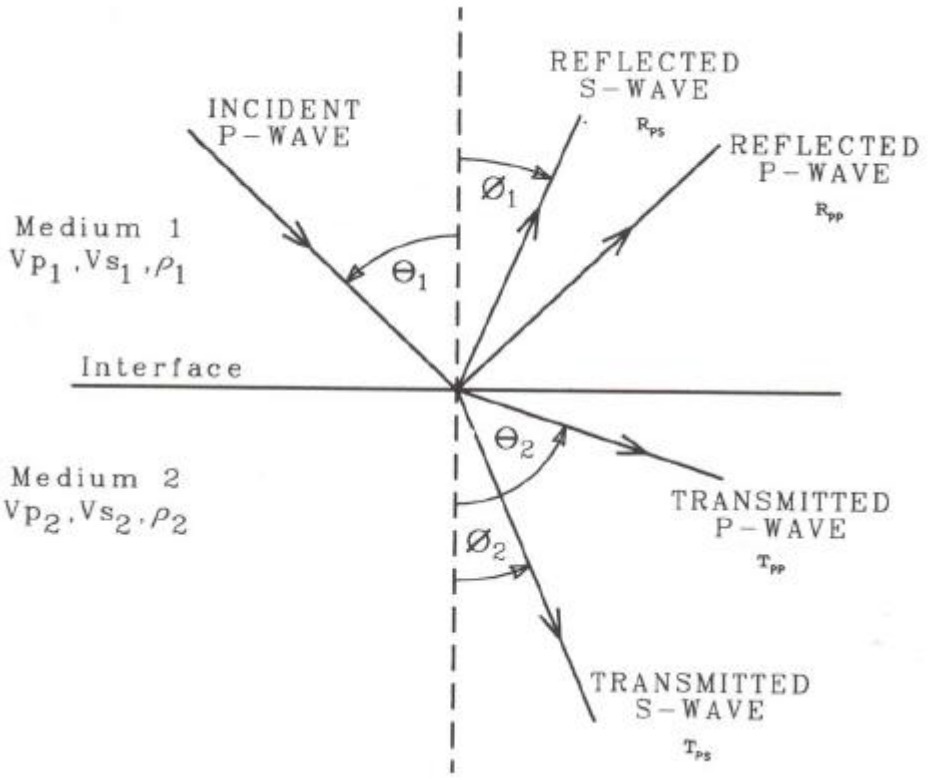

Fig 2. Reflection and transmission at an interface between two infinite elastic half-spaces for an incident P-wave (Castagna et al, 1993).

The P-wave reflection coefficient as a function of incidence angle $R_{PP}(\theta_1)$ is defined as the ratio of the amplitude of the reflected P-wave to that of the incident P-wave. Similarly, the P-wave transmission coefficient $T_{PP}(\theta_1)$ is the is the ratio of the amplitude of the transmitted P-wave to that of the incident P-wave. Also, $R_{PS}(\theta_1)$ is the ratio of the amplitudes of reflected S-wave and incident P-waves, and $T_{PS}(\theta_1)$ is the ratio of the transmitted S-waves amplitudes of transmitted S-waves and incident P-wave amplitudes. The following discussion is for particle displacement amplitudes, with polarity assigned according to the horizontal component of displacement.

At normal incidence, there are no converted S-waves and the P-wave reflection coefficient R_p is given by

$$R_p = \frac{I_{p2} - I_{p1}}{I_{p2} + I_{p1}} = \frac{1}{2}\frac{\Delta I_p}{I_{pA}} = \frac{1}{2} In\left(I_{p2} / I_{p1}\right) \quad \text{..... (3)}$$

Where I_p is the continuous P-wave impedance profile.

I_{p2} = impedance of medium 2 = $\rho_2 V \rho_2$

ρ_2 = density of medium 2.

I_{p1} = Impedance of medium 1 = $\rho_2 V \rho_2$

ρ_1 = density of medium 1.

I_{pA} = average impedance across the interface = ($I_{p2} + I_{p1}$), *and,*

$$\Delta I_p = I_{p2} - I_{p1} \quad \text{..... (4)}$$

The logarithmic approximation is acceptable for reflection coefficients smaller than about + 0.5.

The P-wave transmission coefficient at normal incidence T_p is given by

$$T_p = 1 - R_p. \quad \text{..... (5)}$$

The variation of reflection and transmission coefficients with incident angle (and corresponding increasing offset) is referred to as offset-dependent-reflectivity and is the fundamental basis for amplitude-versus-offset analysis (Castagna et al, 1993).

Knott (1899) and Zoeppritz (1919) invoked continuity of displacement and stress at the reflecting interface as boundary conditions to solve for the reflection and transmission coefficients as functions of incident angle and the elastic properties of the media (densities, bulk and shear moduli), though the resulting Knott and Zoeppritz equations are notoriously complex. Aki and Richards (1980) and Waters (1981) gave an easily solved matrix form

$$Q = P^{-1}R \quad \text{..... (6)}$$

Where Q, P, and R in Appendix A (Castagna and Backus, 1993).

In 1995, Koefoed first showed the practical possibilities of using AVO analysis as an indicator of Vp/Vs variations and empirically established five rules, which were later verified by shuey in 1985 for moderate angles of incidence (Zhang et al, 2001):

a) When the underlying medium has the greater longitudinal [P-wave] velocity and other relevant properties of the two strata are equal to each other, and increase of Poisson's

ratio for the underlying medium causes an increase of the reflection coefficient at the larger angles of incidence.

b) When, in the above case, Poisson's ratio for the incident medium is increased, the reflection coefficient at the larger angles of incidence is thereby decreased.

c) When, in the above case, Poisson's ratio for both media are increased and kept equal to each other, the reflection coefficient at the larger angles of incidence is thereby increased.

d) The effect mentioned in (1) becomes more pronounced as the velocity contrast becomes smaller.

e) Interchange of the incident and the underlying medium affects the shape of curves only slightly, at least up to values of the angle of incidence of about 30 degrees.

In 1961, Bortfeld linearized the Zoeppritz equations by assuming small changes in layer properties $(\nabla\rho/\rho, \nabla V_p/V_p, \nabla V_s/V_s << 1)$ ..... **(7)**

This approach was followed by Richards and Frasier (1976) and Aki and Richards (1980) who derived a form of approximation simply parameterized in terms of the changes in density, P-wave velocity, and S-wave velocity across the interface:

$$R_{pp}(\theta) \approx \frac{1}{2}\left(1 - 4p^2V^2\right)\left\{\frac{\Delta\rho}{\rho}\right\} + \frac{1}{2\cos^2(\theta)} \cdot \frac{\Delta V_p}{V_p} - 4V_s^2\rho^2\,\frac{\Delta V_s}{Vs} \quad \text{..... (8)}$$

Where $\Delta\rho = \rho_2 - \rho_1, \quad \Delta V_p = V_2 - V_1, \quad \Delta V_p = V_2 - V_1, \quad \rho = (\rho_2 + \rho_1)/2.$

$V_p = (V_{p2} + V_{p1})/2, \qquad V_s = (V_{s2} + V_{s1})/2, \quad \theta = (\theta_1 + \theta 2)/2,$

And p is the ray parameter as defined by equation (2). By simplifying the Zoeppritz equations, Shuey (1985) presented another form of the Aki and Richards (1980) approximation,

$$R(\theta) \approx R_o + \left[A_o R_o + \frac{\Delta\sigma}{(1-\sigma)^2} \right] \sin^2\theta + \frac{1}{2}\frac{\Delta V_p}{V_p}\left(\tan^2\theta - \sin^2\theta\right) \quad \text{..... (9)}$$

Where $R_{0\ is}$ the normal-incidence P-P reflection coefficient, A_0 is given by:

$$A_o = B_o - 2(1+B_o)\frac{1-2\sigma}{1-\sigma} \quad \text{..... (10)}$$

And

$$B_o = \frac{\Delta V_p / V_p}{\Delta V_p / V_p + \Delta\rho/\rho} \quad \text{..... (11)}$$

Where

$\Delta\sigma = \sigma_2 - \sigma_1$ And $\sigma = (\sigma_2 + \sigma_1)/2$

The quantity A_0, given by equation (10) above, specifies the variation of R (θ) in the approximation range $0< \theta < 30^{\circ}$ for the case of no contrast in Poisson's ratio. The first term gives the amplitude at normal incidence, the second term characterizes R (θ) at intermediate angles, and the third term describes the approach to the critical angle (Castagna et al, 1993).

The coefficients of Shuey's approximation form the basis of various weighted procedures. "Weighted stacking", here also called "Geostack" (Smith and Gidlow, 1987), is a means of reducing prestack information to AVO attribute traces versus time. This is accomplished by

calculating the local angle of incidence for each time sample, the performing regression analysis to solve for the first two or all three coefficients of an equation of the kind:

$$R(\theta) = A + B\sin^2\theta + C\sin^2\theta\tan^2\theta \quad \text{..... (12)}$$

Where A is the "Zero-offset" stack, B is commonly referred to as the AVO "slope" or "gradient", and the third term becomes significant in the far-offset stack (Zhang et al, 2001).

2.3 REFLECTION COEFFICIENTS OF AN INTERFACE

In 1940, a classic article was published by Muskat and Meeres showing the variations in plane-wave reflection and transmission coefficients as a function of angle of incidence. Since then, several additional articles on the subject have appeared in the literature, including those by Koefoed (1955, 1962) and Tooley et al. (1965), one can show that four independent variables exist at a single reflecting/refracting interface between two isotropic media: 1) P-wave velocity ratio between the two bounding media; 2) density ratio between the two bounding media; 3) Poisson's ratio in the upper medium; and 4) Poisson's ratio in the lower medium. These four quantities govern plane-wave reflection and transmission at a seismic interface. Since Muskat and Meres (1940) had very little information on values of Poisson's ratios for sedimentary rocks, they used a constant value of 0.25 in all their calculation, i.e., Poisson's ratio was the same for both media. Results similar to theirs are shown in Figure 3 below for various velocity and density ratio and constant Poisson's ratios of 0.2 and 0.3. One would conclude from these results that angle of incidence has only minor effects on P-wave reflection coefficients over propagation angles commonly used in reflection seismology. This is a basic principle upon which conventional common-depth-point (CDP) reflection seismology relies (Ostrander 1984).

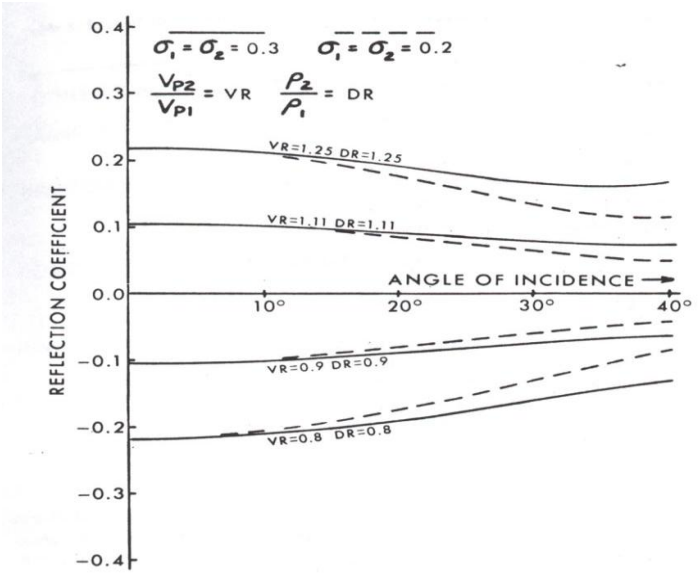

Fig. 3 Plot of P-wave reflection coefficient versus angle of incidence for constant Poisson's ratio of 0.2 and 0.3 (Ostrander 1984).

The work of Koefoed (1955) is of particular interest since his calculations involved a change in Poisson's ratio across the reflecting interface. He found that by having substantially different Poisson's ratio for the two bounding media, large change in P-wave reflection coefficients versus angle of incidence could result. Koefoed showed that under certain circumstances, reflection coefficients could increase substantially with increasing angle of incidence. This increase occurs well within the critical angle where high-amplitude, wide-angle reflections are known to occur. Figures 4 and 5 illustrate an extension of Koefoed's initial computations. Figure 3 shows P-wave reflection coefficients from an interface, with the incident medium having a higher Poisson's ratio than the underlying medium. The solid curves represent a contrast in Poisson's ratio of 0.4 to 0.1, while the dashed curves represent a contrast of 0.3 to 0.1. It can be deduced from the curves that Poisson's ratio decreases towards the underlying medium, the reflection coefficient decreases algebraically with increasing angle of incidence. This means positive reflection

coefficients may reverse polarity and negative reflection coefficients increase in magnitude (absolute value) with increasing angle of incidence (Ostrander 1984).

Figure 5 shows the opposite situation to that shown in Figure 4. Here Poisson's ratio increases going from the incident medium into the underlying medium. In this case, the reflection coefficient increases algebraically with increasing angle of incidence. Negative reflection coefficients may reverse polarity, and positive reflection coefficients increase in magnitude with increasing angle of incidence. The foregoing three illustrations point to a strong need for more information on Poisson's ratio for the various rock types encountered in seismic exploration. This is particularly important when one considers the long offsets commonly in use today and the resulting large angles of incidence. More information on computations of reflection and transmission coefficients can be found in Koefoed (1962) and (Tooley et al. 1965).

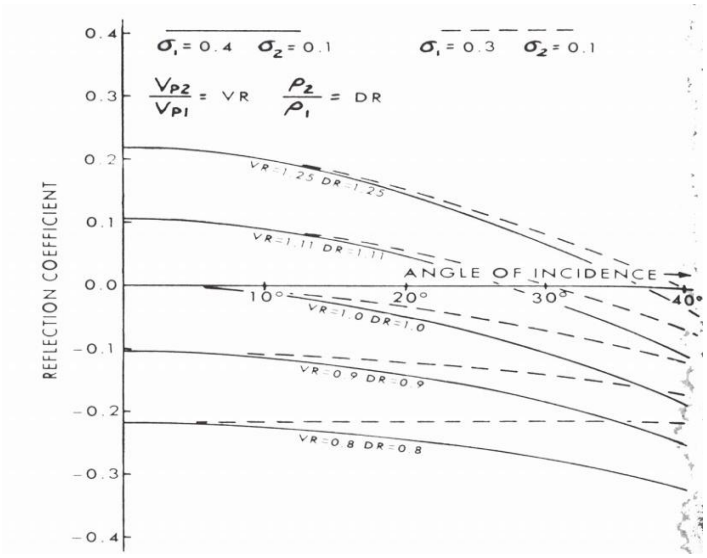

Fig 4. Plot of P-wave reflection coefficient versus angle of incidence for a reduction in Poisson's ratios across an interface (Ostrander 1984).

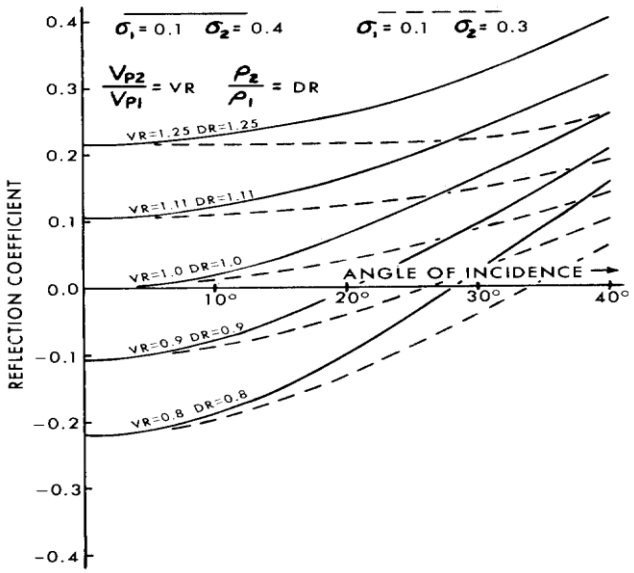

Fig 5. Plot of P-wave reflection coefficient versus angle of incidence for a increase in Poisson's ratios across an interface (Ostrander 1984).

2.4 APPROXIMATION TO THE KNOTT AND ZOEPPRITZ EQUATIONS

The unwieldy nature of Knott-Zoeppritz equations defies the physical insight, which forms the visualization of how the variation of a particular parameter will affect the reflection coefficient curve. Approximations are extremely useful for practical applications as they readily brings out the information in the amplitude behavior, which do not require computer to evaluate and provide the basis for certain AVO processing techniques (Castagna et al, 1993).

2.4.1 LINEAR APPROXIMATION OF ZOEPPRITZ'S EQUATION.

Zoeppritz's equation are implicitly coupled to the various rock properties of interest and do not provide any direct interpretive insight to the AVO behavior. For this reason, linear approximation of Zoeppritz's equation were developed to explicitly relate rock properties

thereby providing interpreters with a more direct understanding of AVO anomalies(Wardhana, 2001).

In 1961, Bortfeld linearized the Zoeppritz equations by assuming small changes in layer properties and obtained

$$R_{pp}(\theta_1) \approx \frac{1}{2} In\left[\frac{V_{p2\rho 2}\cos\theta_1}{V_{p1\rho 1}\cos\theta_2}\right] + \left(\frac{\sin\theta_1}{V_{p1}}\right)^2 \left(V_{s1}^2 - V_{s2}^2\right) \times \left[2 + \frac{In\left(\frac{\rho_2}{p_1}\right)}{In\left(\frac{V_{s2}}{V_{s1}}\right)}\right] \quad \text{..... (13)}$$

In 1976, Richards and Fraiser also followed the same approach and Aki and Richards also followed suite in 1980. They derived a form simply parameterized in terms of the changes in density, P-wave velocity, and S-wave velocity across the interface.

2.4.2 REFLECTION COEFFIECIENT BASED ON ZOEPPRITZ'S EQUATION.

In this section, an introduction of a formula of reflection coefficient developed by Zoeppritz in 1999 is illustrated. This is usually used in computing the AVO response from channel models. Consider a plane wave travelling into the earth with an angle θ, that is incident onto an interface separating two different rocks having properties (α_1, β_1, ρ_1 and α_2, β_2, ρ_2), and is then recorded by a receiver on the earth's surface in Fig 6 (Wardhana, 2001).

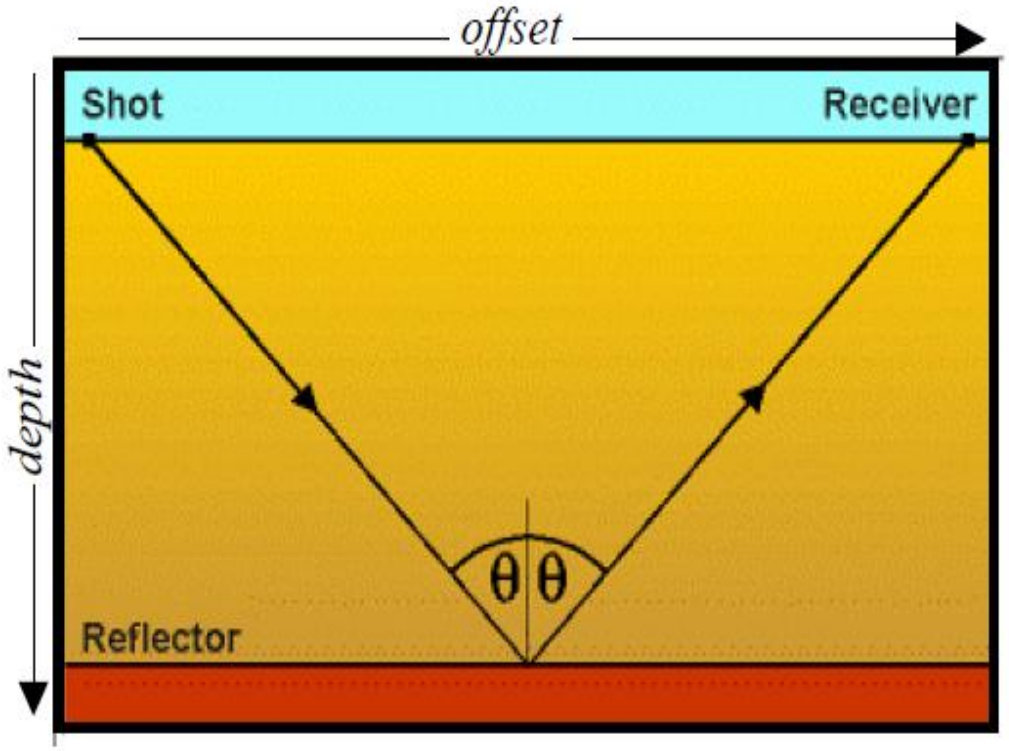

Fig. 6 The seismic experiment (Wardhana, 2001).

The mathematical expression for the reflection of down going P and up going P waves derived by Cerveny and Ravindra in 1971 is given below.

$$RC_{pp} = -1 + 2P_1 D^{-1}\left(\alpha_2\beta_2 P_2 X^2 + \beta_1\alpha_2\rho_1\rho_2 P_4 + q^2\Theta^2 P_2 P_3 P_4\right) \quad \text{..... (14)}$$

Where

$$D = \alpha_1\alpha_2\beta_1\beta_2\Theta^2 Z^2 + \alpha_2\beta_2 P_1 P_2 X^2 + \alpha_1\beta_1 P_3 P_4 Y^2 + \rho_1\rho_2\left(\beta_1\alpha_2 P_1 P_4 + \alpha_1\beta_2 P_2 P_3\right) + q^2\Theta^2 P_1 P_2 P_3 P_4, \quad \text{.... (15)}$$

And

$$q = 2\left(\rho_2\beta_2^2 - \rho_1\beta_1^2\right) \quad \text{..... (16)}$$

$$X = \rho_2 - q\Theta^2, \quad Y = \rho_1 + q\Theta^2, \quad Z = \rho_2 - \rho_1 - q\Theta^2, \quad \Theta = \sin\theta_1 / v_1 \quad v_1 = \alpha_1$$

$$v_2 = \beta_1, \quad v_3 = \alpha_2, \quad v_4 = \beta_2, \quad P_i = (1 - v_i^2\Theta^2)^{1/2} \ (i = 1,2,3,4)$$

The importance of the formulation above is that it closely fits Zoeppritz's equations. The only disadvantage of this long mathematical expression is that one can hardly understand the direct impact on rock-properties on reflection coefficients (Wardhana, 2001).

2.5 CONSTITUTIVE RELATIONS OF A POROUS MEDIA

Multiphase porous media embedded with a phase-change constituent have been found in numerous engineering applications, e.g., binary alloy solidification, self-healing composites, adaptive energy-absorbing foams, freeze-thaw soils, sea ice, and musculoskeletal and skin tissues. These material, typically characterized by multiphase, multi-length scales, complicated microstructure evolution process and phase-change mechanisms, are classified as "porous media". Poroelasticity theory pioneered and developed by Terzaghi (1923, 1925) and Biot (1935, 1941, 1955, and 1962) has been used to find mechanics solutions for various porous media. The poroelasticity theory has been used to obtain analytical solutions and computational schemes including finite element and boundary element solutions to problems related to soil consolidation (Lewis and Schrefler, 1987), offshore geotechnique (Madsen, 1978; Cheng and Liu, 1986), hydraulic fracturing for energy resource exploration (Detournay and Cheng, 1991) and estimation of subsidence due to fluid withdrawal or have due to fluid injection (Verruijt, 1969). The theory has also found extensive applications in biomechanics of soft tissues and cells, mechanics of bone, transport of multiphase fluids in porous media, especially in environmental geomechanics and energy resource recovery, earthquake, and in the study of advanced materials

such as saturated micro-cellular foams, polymer composites, and smart materials. The applications have resulted in the modification of classical poroelasticity theory to include more complex phenomena in the description of both the porous skeleton and the interstitial fluid (Zhang, 2008).

The formulation of the constitutive equations for porous media in poroelasticity theory is based on linear elasticity and on macroscopic scale without explicitly including the contributions from solid skeleton and fluid constituents. The local portions of each constituent of the media are counted by the measure of volume fractions and the degree of saturation. It is thus essential to use micro-mechanics in obtaining the constitutive relation of multiphase porous media involving phase-change process to elicit the dependence of the bulk material coefficients on the mechanical properties and structures of each constituent at microscopic scale (Zhang, 2008).

2.6 CONSTITUTIVE RELATION

The macroscopic stresses of the multiphase porous media are calculated from the microscopic stresses using homogenization scheme, which is a volume average of the microscopic stresses within the representative unit cell and are given by

$$\sum ij = \frac{1}{V}\int_v \sigma_{ij} dv \qquad \text{..... (17)}$$

The macroscopic strain for porous solids is calculated by the following equation which is given by Bishop and Hill (1951).

$$\sum ij = \frac{1}{V}\int_v \sigma_{ij} dv + \frac{1}{2V}\int s_{voids}\left(u_i n_j + u_j n_i\right) ds \quad \text{..... (18)}$$

Where n_i is the unit outward normal vector of the surfaces (Zhang, 2008).

2.7 GASSMAN FLUID SUBSTITUTION

The mechanics of fluid substitution is an important part of the seismic rock physics analysis (e.g., AVO, 4D analysis), which provides a tool for fluid identification and quantification in reservoir. This is commonly performed using Gassmann's equation (Gassmann, 1951). Other authors like (Batzle and Wang, 1992; Berryman, 1999; Wang, 2001; Smith et al., 2003; Russell et al., 2003; Han and Batzle. 2004) have discussed the formulations, strength and limitations of the Gassmann fluid substitution. However detailed discussions on this subject have not been fruitful (Kummar, 2006).

The objective of Gassmann's fluid substitution is to model the seismic properties(seismic velocities) and density of a reservoir at a given reservoir condition(e.g., pressure, temperature, porosity, mineral type and water salinity) and pore fluid saturation such as 100% water saturation or hydrocarbon with only oil or only gas saturation. Seismic velocity of an isotropic material can be estimated using known rock moduli and density. P-and S-wave velocities in isotropic media are estimated as,

$$V_P = \sqrt{\frac{K + 4\mu/3}{\rho}} \quad \text{..... (19)}$$

And

$$V_s = \sqrt{\frac{\mu}{\rho}} \quad \text{..... (20)}$$

Respectively, where V_P and V_s are the P-and S-wave velocity, K and μ are the bulk and shear moduli, and ρ is the mass density. Density of saturated rock can be simply computed with the volume averaging equation (mass balance). Other parameters required to estimate seismic velocities after fluid substitution are the moduli and, which can be computed using the Gassmann's equations (Kumar, 2006).

2.7.1 GASSMANN'S EQUATIONS

Gassman's equations relate the bulk modulus of a rock to its pore, frame and fluid properties. The bulk modulus of a saturated rock is given by the low frequency Gassmann theory (Gassman, 1951) as

$$K_{sat} = K_{frame} + \frac{\left(1 - \frac{K_{frame}}{K_{matrix}}\right)}{\frac{\phi}{K_{fl}} + \frac{(1-\phi)}{K_{matrix}} - \frac{K_{frame}}{K_{matrix}^2}} \quad \text{..... (21)}$$

Where, K_{frame}, K_{matrix}, K_{fl} are the bulk moduli of the saturated rock, porous rock frame (drained of any pore-filling porosity (as fraction). In the Gassmann formulation shear modulus is independent of the pore fluid and held constant during the fluid substitutions. Bulk modulus (K_{sat}) and shear modulus (μ) at in-situ (or initial) condition can be estimated from the wireline log data (seismic velocities and density) by rewriting equations 1 and 2 as

$$K_{sat} = r\left(V_p^2 - \tfrac{4}{3}V_s^2\right) \quad \text{..... (22)}$$

And

$$\mu = \rho V_s^2 \quad \text{..... (23)}$$

To estimate the saturated bulk modulus (equation 22) at a given reservoir condition and fluid type we need to estimate bulk moduli of frame, matrix and pore fluid (Kumar, 2006).

2.7.2 FLUID PROPERTIES

Bulk modulus and density of the pore fluid (brine, oil and gas) are estimated by averaging the values of individual fluid type. Let's first consider properties of each fluid type (brine, gas, and oil)

i) Bulk modulus and density of brine

The seismic velocity and density of brine can be used to estimate it's Bulk modulus.

i.e. $K_{brine} = \rho_{brine} V_{brine}^2 \times 10^{-6}$ ..... **(24)**

Where $K_{brine}(GPa)$, $\rho_{brine}(g/cm^3)$ and $V_{brine}(m/s)$ are the bulk modulus, density and P-wave velocity in brine. Units are given in the brackets. Brine composition can range from almost pure water to saturated saline solution (characterized by the salinity). Density and velocity in brine can be calculated following Batze and Wang (1992). Density of brine is given by

$$\rho_{brine} = \rho_{\omega} + 0.668S + 0.44S^2 + 10^{-6}S\left[300P - 2400PS + T\left(80 + 3T - 3300S - 13P + 47PS\right)\right] \quad \text{..... (25)}$$

Where $P(MPa)$ and $T^{o}(C)$ are the in-situ pressure and temperatures, S (as weight fraction) is the salinity of brine, $\rho_{\omega}(g/cm^3)$ is density of water given by

$$\rho_{\omega} = 1 + 10^{-6}\left(-80T - 3.3T^2 + 0.00175T^3 + 489P - 2TP + 0.016T^2P - 1.3\times10^{-5}T^3P - 0.333P^2 - 0.002TP^2\right) \quad \text{..... (26)}$$

P-wave velocity of brine, $V_{brine}(m/s)$ is given as

$$V_{brine} = V_{\omega} + S\left(1170 - 9.6T + 0.055T^2 - 8.5\times10^{-5}T^3 + 2.6P - 0.0029TP - 0.0476P^2\right) + S^{1.5}\left(780 - 10P + 0.16P^2\right) - 1820S^2 \quad \text{... (27)}$$

Where $V_{\omega}(m/s)$ is P-wave velocity in pure water. This can be estimated by

$$V_{\omega} = \sum_{i=1}^{5}\sum_{j=1}^{4} \omega_{ij} T^{i-1} P^{j-1} \quad \text{..... (28)}$$

Where ω_{ij} constants.

ii) BULK MODULUS AND DENSITY OF GAS

Bulk modulus and density of a gas in a reservoir depend on the pressure, temperature and the type of gas, Hydrocarbon gas can be a mixture of many gases, and they are characterized by specific gravity G, the ratio of the gas density to air density of $15.6^{o}C$ and atmospheric pressure. Following Batzle and Wang (1992) density of gas can be estimated as

$$\rho_{gas} \cong \frac{28.8GP}{ZR(T + 273.15)} \quad \text{..... (29)}$$

Where G is the specific gravity of gas (API), R is the gas constant (8.314) and Z is the compressibility factor given by:

$$Z = \left[0.03 + 0.00527(3.5 - T_{pr})^3\right]P_{pr} + \left(0.642T_{pr} - 0.007T_{pr}^4 - 0.52\right) + E \quad \text{..... (30)}$$

And

$$E = 0.109(3.85 - T_{pr})^2 \exp\left\{-\left[0.45 + 8\left(0.56 - 1/T_{pr}\right)^2\right]P_{pr}^{1.2} \Big/ T_{pr}\right\} \quad \text{..... (31)}$$

In the above equation, T_{pr} and P_{pr} are the pseudo-reduced temperature and pressure, respectively, and are given by

$$T_{pr} = \frac{T + 273.15}{94.72 - 170.75G} \quad \text{..... (32)}$$

The bulk modulus of gas (GPa) is given by (Batzle and Wang, 1992)

$$K_{gas} \cong \frac{P}{\left(1 - \frac{P_{pr}}{Z}\frac{\partial Z}{\partial P_{pr}}\right)_T}\frac{\gamma_o}{1000} \quad \text{..... (33)}$$

iii) BULK MODULUS AND DENSITY OF OIL

Oil contains some dissolved gas characterized by the GOR (gas-to-oil ratio) value. Similar to gas, oil, density and bulk modulus depend on the temperature, pressure, GOR and the type of oil. Density and velocity in oil can be written following Batzle and Wang (1992) and Wang (2001) as,

$$\rho_{oil} = \frac{\rho_s + \left(0.00277P - 1.71\times10^{-7}P^3\right)\left(\rho_s - 1.15\right)^2 + 3.49\times10^{-4}P}{0.972 + 3.81\times10^{-4}(T + 17.78)^{1.175}} \quad \text{..... (34)}$$

And

$$V_{oil} = 2096\sqrt{\frac{\rho_{ps}}{2.6 - \rho_{ps}}} - 3.7T + 4.64P + 0.0115\left[\sqrt{\frac{18.33}{\rho_{ps}}} - 16.97 - 1\right]TP \quad \text{..... (35)}$$

Where $\rho_{oil}(g/cm^3)$ and $V_{oil}(m/s)$ are the density and P-wave velocity in oil (containing some dissolved gas). In the above equations, ρ_s and ρ_{ps} are the saturation density and pseudo density given as

$$\rho_s = \frac{\rho_o + 0.0012R_G G}{B_o} \quad \text{..... (36)}$$

And

$$\rho_{ps} = \frac{\rho_o}{(1 + 0.001R_G)B_0} \quad \text{..... (37)}$$

Where R_G is the GOR (litre/litre), $\rho_o(g/cm^3)$ is the reference density of oil measured at 15.6^{o}C and atmospheric pressure and is called the formation volume factor which is given by the formula

$$B_o = 0.972 + 0.00038\left[2.495R_G\sqrt{\frac{G}{\rho_o}} + T + 17.8\right]^{1.175} \quad \text{..... (38)}$$

Once velocity and density are known, bulk modulus of oil, $K_{oil}(GPa)$ can be calculated as

$$K_{oil} = \rho_{oil}V_{oil}^2 \times 10^{-6} \quad \text{..... (39)}$$

Fluid in the pore spaces consists of brine and hydrocarbon (oil and /or gas). Bulk modulus and density of the mixed pore fluid phase can be estimated by inverse bulk modulus averaging (also known as Wood's equation) and arithmetic averaging of densities (i.e., mass balance) of the separate fluid phases, respectively. Bulk modulus (K_{fl}) and density ρ_{fl} of the fluid phase are given as

$$\frac{1}{K_{fl}} = \frac{WS}{K_{brine}} + \frac{HS}{K_{hyc}} \quad \text{..... (40)}$$

And

$$\rho_{fl} = WS\rho_{brine} + HS\rho_{hyc} \quad \text{..... (41)}$$

Where WS is the water saturation (as fraction) and HS (= 1 –WS) is the hydrocarbon saturation, K_{hyc} and ρ_{hyc} are the bulk modulus and density of hydrocarbon, respectively, In the case of oil as hydrocarbon,

$$K_{hyc} = K_{oil} \quad \text{..... (42)}$$

And

$$\rho_{hyc} = \rho_{oil} \quad \text{..... (43)}$$

And in the case of gas as hydrocarbon,

$$K_{hyc} = K_{gas} \quad \text{..... (44)}$$

And

$$\rho_{hyc} = \rho_{gas} \quad \text{..... (45)}$$

2.7.3 FRAME PROPERTIES

Frame bulk modulus can be derived from the laboratory measurement, empirical relationship, or wireline log data. When working with wire line data, K_{frame} can be determined by rewriting the Gassmann equation (equation 20) for K_{frame} (Zhu and McMechan, 1990) as

$$K_{frame} = \frac{K_{sat}\left(\frac{\phi K_{matrix}}{K_{fl}} + 1 - \phi\right) - K_{matrix}}{\frac{\phi K_{matrix}}{K_{fl}} + \frac{K_{sat}}{K_{matrix}} - 1 - \phi} \quad \text{..... (46)}$$

All the parameters in the above equation (36) are known from the previous formulation: $K_{sat}(equation\,4)$, $K_{matrix}(equation\,6)$, $K_{fl}(equation\,30)$. The K_{frame} value remains unchanged during fluid substitution.

2.7.4 MATRIX PROPERTIES

To calculate the bulk modulus of mineral matrix, one needs to know the mineral composition of rock. This can be found from laboratory examination of core samples. Litho logy can be assumed to be a composition of quartz and clay minerals in the absence of laboratory data. The percentage of clay can be derived from the volume shale (V_{sh}) curve, which is typically derived from the wire log data (Gamma-ray log). Typical shale contains about 70% of clay and 30% of other minerals (mostly quartz). Once the mineral abundances are determined, K_{matrix} can be calculated via the application of Voigt-Reuss-Hill (VRH) averaging (Hill, 1952) of the mineral constituents. Input for K_{matrix} calculation are V_{sh}, K_{clay} (bulk modulus of clay), K_{qtz} (bulk modulus of quartz). The K_{matrix} can be calculated by the VRH averaging as

$$K_{matrix} = \frac{1}{2}\left(\left[V_{clay}K_{clay} + V_{qtz}\right] + \left[\frac{V_{clay}}{K_{clay}} + \frac{V_{qtz}}{K_{qtz}}\right]\right) \quad \text{..... (47)}$$

Where V_{clay} and V_{qtz} are

V_{clay} = 70% V_{sh} (this is an assumption)

And

$V_{qtz} = 1- V_{clay}$

Density of the mineral matrix ρ_{matrix} can be estimated by arithmetic averaging of densities of individual minerals as

$$\rho_{matrix} = V_{clay}\rho_{clay} - V_{atz}\rho_{qtz}$$

Where ρ_{clay} and ρ_{qtz} are the density of the clay and quartz minerals. Bulk moduli of clay (20.9GPa) and quartz (36.6Gpa), and densities of clay (2.58g/cm^3) and quartz (2.65 g/cm^3) can be found in text books (e.g., Mavko, Mukerji and Dvorkin, 1998) or from the core analysis in the laboratory. The values of K_{matrix} and ρ_{matrix} remain constant during the Gassman fluid substitution.

CHAPTER 3

METHODOLOGY

3.1 INTRODUCTION

The science of seismology began with the study of naturally occurring earthquakes. Seismologists at first were motivated by the desire to understand the destructive nature of large earthquakes. They soon learned however that the seismic waves produced by an earthquake contained valuable information about the large-scale structures of the Earth interior. Today, a much of our understanding of the Earth mantle crust and core is based on the analysis of the seismic waves produced by earthquakes. Thus seismology became an important branch of geophysics, which is the physics of the Earth (Brian, 1997).

Seismologists and geologists also discovered that similar but much weaker man-made seismic waves had a more practical use. They could probe the very shallow structure of the Earth to help locate its mineral water and hydrocarbon resources, thus the seismic exploration industry was born and the seismologists working in that industry came to be called exploration geophysicist. Today seismic exploration encompasses more than just the search for resources. Seismic technology is used in the search for waste-disposal sites in determining the stability of the ground under proposed industrial facilities and even in archaeological investigations. Nevertheless, since hydrocarbon exploration is still the reason for the existence of the seismic exploration industry, the methods and terminology explained related to seismic are commonly used in the oil and natural gas exploration industry. The underlying concept of seismic exploration is simple Man-made seismic waves are just waves (also called acoustic waves) with

frequencies typically ranging from about 5Hz to just over 100Hz. (The lowest sound frequency audible to the human ear is about 30Hz). As these sound waves leave the seismic source and travel downward into the Earth, they encounter changes in the Earths geological layering which cause echoes (or reflections) to travel upward to the surface Electromechanical transducers (geophones or hydrophones) detect the echoes arriving at the surface and convert them into electrical signals which are then amplified, filtered, digitized an recorded. The recorded seismic data usually undergo elaborate processing by digital computers to produce images of the earth's shallow structure. An experienced geologist or geophysicist can interpret those images to determine what type of rocks they represent and whether those rocks might contain valuable resources (Brian, 1997).

It is commonly assumed that a stacked seismic trace is the convolution of a wavelet and a vertical incidence reflection coefficient series. In reality seismic energy in a shot record strikes any given boundary with a wide range of incidence angles resulting in P to S wave conversion. It is easily shown in the resulting reflection coefficient depends on P-wave velocity, S-wave velocity and layer density and the variation of P-wave reflected amplitude with angle of incidence (or offset) depends on Poisson's ratio and density contrasts between layers. Various authors including shuey (1985) have published simplified approximations of the full Zoeppritz equations. The AVO response equation at a boundary between two layers is commonly expressed as:

$$R(\theta) = R_o \cos^2 \theta + \{\Delta\sigma/(1-\sigma)^2\}\sin^2 \theta \quad \text{..... (48)}$$

Where R (θ) is the reflection coefficient at angle of incidence θ, σ is Poisson's ratio and R_o is the reflection coefficient at zero offset.

Note that this two term equation is valid only up to 30 degrees angle of incidence. The two terms tell us that the AVO response is dominated by R_o at small angles and the contrast in Poisson's ratio at large angles. The equation also tells us that an increase in Poisson's ratio across the boundary will cause an increase in reflected amplitude with angle of incidence and vice versa. So intuitively, an interface may show a positive, negative or zero $R_{o,}$ and the amplitude may either increase or decrease with offset. This leads so far, to six potential observations on a seismic gather (McGregor, 2007).

High amplitude reflections associated with the boundary between gas-bearing zones (sands) and cap rocks (shale) are routinely referred to as "bright spots" (Khattri et al, 1979). Offset dependent reflection amplitude (Amplitude Versus Offset [AVO] characteristics for gas rich sediments can vary significantly with geologic setting, gas concentrations, and lithology (Ostrander, 1982). Three unique types of reservoirs or classes of gas deposits have been described that incorporate geology setting and lithology with seismic attributes (Rutherford and Williams, 1989). Lithologically, the encasing medium or mechanism and reservoir rock distinguish these classes while seismically, a distinct impedance range aids in classifying each type of gas sand (Begay et al, 2000).

3.2 WHAT ARE SEISMIC DATA

Seismic data is generated by using vibrations to capture a two-dimensional picture of the rock layers beneath the surface. The interpretation of seismic data allows the scientist to make an

estimated picture of the rocks beneath the surface without drilling or digging trenches. The collection of vibrations which, when coupled with time elements, represent the rate of transmission of energy through a material. Scientist have measured many different materials and have a portfolio of data which allow them to interpret the type of material, the structure of the material, and the depth below the surface of the material, all based upon the nature of the vibrations. The data are used in many ways, from determining how thick the soil may be in an area, to locating cracks in the rocks.

3.2.1 BACKGROUND OF THE INVENTION

Seismic surveys are conducted for the purpose of investigating and modeling the depth and structure of subsurface earth formations as a preliminary activity in exploiting natural resources. During the course of reflection seismometry, a source, emplaced at or near the surface of the earth, radiates an acoustic wavefield. The wavefield may be created by an impulsive source, by a chirp-signal generator or any other means now known or unknown. The wavefield propagates downwardly into the earth to insonify the earth strata below. The wavefield is reflected from the respective subsurface strata back to the surface where the mechanical motions of the seismic waves are converted to electrical signals by seismic sensors such as geophones or accelerometers. The received, reflected seismic signals may be recorded and processed by means well known to the art such as by computer, to provide and display a multi-dimensional model. Seismic studies may be performed in one dimension to provide a single time-scale trace exhibiting a desired seismic parameter as a simple function of time (or depth if the propagation velocity of seismic waves is known). The data are generated using a substantially single source

and a substantially single sensor which may be, for example lowered to various levels in a borehole as in vertical seismic profiling (VSP) (Lapucha, 1994).

Seismic surveys may be conducted in two dimensions (2-D) wherein a plurality of sensors, such as for example, 100 are distributed at spaced-apart interval, commonly known to the industry as a spread, along a designated line of survey at or near the surface of the earth. Each sensor or compact group of several interconnected sensors is coupled by a signal transmission means to a dedicated signal-conditioning and recording channel. Seismic sensors receive the wavefield after reflection from the earth formations below. The electrical signals resulting from the reflected waveforms may be recorded, processed and formatted as a plurality of time-scale traces. The time-scale traces provide an analog of a cross section of the earth along a single vertical plane having the dimensions of reflection travel time vertically, and offset distance horizontally. After each shot, source and sensors are progressively advanced along the line of survey by a preselect incremental distance until the entire length of the survey line has been occupied (Lapucha, 1994).

Three dimensional (3-D) surveys may be conducted wherein many hundreds or thousands of seismic sensors are distributed aerially over an extended region in a grid pattern of sensor stations established with reference to north and east geographic coordinates. Typical grid dimensions might be on the order of 50 by 100 meters. A 3-D survey is capable of providing a model of a volumetric cube of the sub-surface earth strata. Each sensor or sensor group is connected to a single recording channel. Each time that a source is fired, it insonifes a large patch of sensors. After each firing, the source moves to a new location where the firing is repeated. Three dimensional data acquisition systems depend upon real-time transmission of the seismic data through a multi-channel telemetric system. All of the data are recorded and partially

preprocessed at a central, operator-occupied field recording station, usually trunk-mounted, customarily; the sensors and interconnecting cable are laid out will in advance of the appearance of the central station and source equipment (Lapucha, 1994).

3.3 CLASSIFICATION OF AVO

The original AVO classification scheme proposed by Rutherford and Williams (1989) was limited to gas sands underlying shale which exhibit a subset of the range of possibilities now recognized:

1. Class 1 – High impedance sands
2. Class 2 – near zero impedance contrast sands
3. Class 3 – low impedance sands

High impedance contacts between encasement and sand termed class 1, are mature sand that have been exposed to moderate to high compaction (Rutherford and Williams, 1989). Seismically, reflection amplitudes decrease with offset and may result in a polarity reversal if sufficient offsets are recorded.

Class 2 sand reservoirs posses near-zero impedance contrast between the sand and encasing materials and are moderately compacted sands (Rutherford and Williams, 1989). This type of gas sand has very low amplitude reflections at near offsets and significantly higher amplitude reflections at far offsets. This offset-dependent seismic response is opposite from “normal”

seismic response, therefore processing flows designed for average earth materials are rarely effective in detecting the unique characteristics of class 2 gas reservoirs.

The third (3) class of gas sands has lower impedance than the encasing medium and is usually unconsolidated (Rutherford and Williams, 1989). Seismically, reflections appear at offset ranges and without polarity changes. In some cases, deeper layers are not imaged due to limited or no transmission of energy through the base of the confining layer (Pullen et al, 1998).

High impedance gas sands show a positive reflection coefficient at the top boundary. The decrease of Poisson's ratio entering the gas sand results in a dimming with offset. Class 3 sand will show a negative reflection coefficient at the top boundary. The decrease in Poisson's ratio causes a further decrease in reflection coefficient with offset; the event gets more negative across the gather resulting in the classic Gulf of Mexico "bright spot".

The AVO response equation expressed above can be simplified further and written as follows for angles of incidence less than 30 degrees; the angular dependence of P-wave reflection coefficients is now expressed in terms of two parameters, the AVO intercept (A) and the AVO gradient (B).

$$R(\theta) = A + B\sin^2\theta \quad \text{..... (49)}$$

Where A represents the normal incidence P-wave reflectivity or intercept term and B is the gradient term containing the AVO effects (McGregor, 2007).

It should now be apparent that amplitudes for any event across a seismic gather can be plotted against incidence angle as shown in Fig. 1. This allows the intercept amplitude to be computed

for any event in the gather and the computation of the zero-offset or intercept stack; this is more representative of the compressional impedance than the full stack in which the amplitude variations with offset are simply averaged out. This in essence is why AVO interpretation has become key; the stacking process is by its very nature designed to average out amplitude variations are caused by changes in Poisson's ratio (which can be directly related to compressional and shear velocities) and density, which the geophysicist wants to relate directly to useful rock properties changes in lithology and fluid (McGregor, 2007).

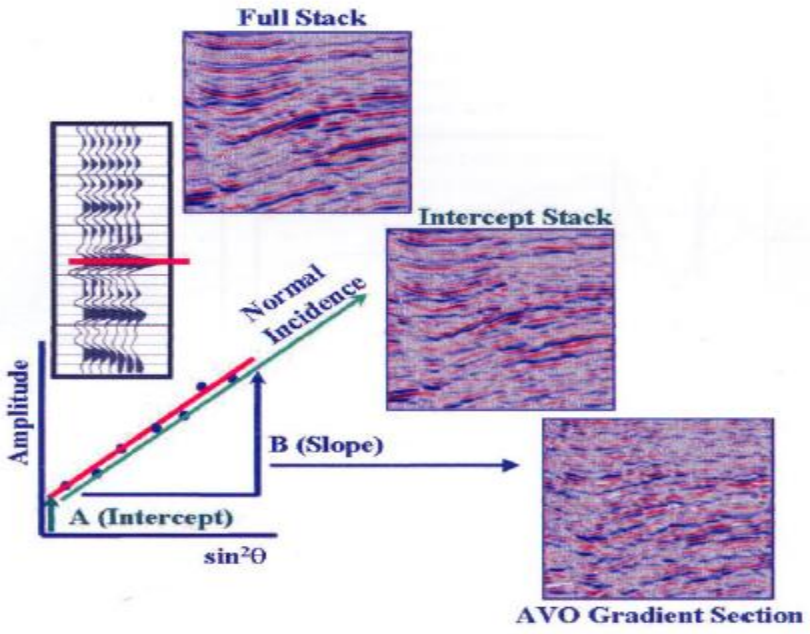

Fig. 7. The derivation of the intercept stack and gradient section. Source (McCregor, 2007)

From the Fig. 6 above, it is also possible to compute the value of gradient B for any particular event in the gather. This leads to the AVO gradient section. The gradient section shows areas

where AVO anomalies are present as high amplitude events. In the absence of a gradient the section is quiescent. The gradient section led directly to the interpretation methods first commonly used in the industry where the gradient section functions as a screening tool. Gathers are examined in those areas high graded from the gradient section analysis. The traditional workflow is then to analyze the events on the gathers by trying to match the response with model gathers.

3.4 METHODS OF ACQUIRING AND PROCESSING SEISMIC DATA

The objective of seismic processing is to manipulate acquired data into an image that can be used to interpret the sub-surface structure. This principle of the seismic reflection profiling technique is deceptively simple. A disturbance at or near surface of the Earth generates elastic waves that propagates through the Earth and are detected and recorded by sensors at the surface near the source. In as much as other kinds of waves are sometimes useful, most information comes from the compressional waves that travel along near-vertical paths and are partially reflected at buried sub-horizontal interfaces between rocks of contrasting impedance. The travel time of a pulse propagating along such a path is perhaps the prime information gathered, but the amplitude, phase, frequency content, and apparent surface velocity of the signal are also valuable(Oliver, 1978).

The source and receivers are moved together along a line and the experiment repeated at closely spaced intervals so that subsurface reflecting horizons may be traced, and a profile or section obtained in a similar manner to that of a marine echo sounder. The velocities along the profile must be known or measured to be used to determine the basic travel-time data that must be ultimately converted to depths and reflectors properly positioned. The velocity is commonly

measured by using the common reflected waves travelling along paths that are somewhat off the vertical. Thus many sensors distributed over a distance ranging from near zero to significant of depths must be detected or recorded by single source of deepest reflecting horizon Moreover, because the sources generates kinds of waves(surface waves, shear waves, waves with complex paths and diffracted waves) in addition to the nearly vertical travelling compressional waves that are normally the signal, arrays of many sources of elements and arrays of many receivers are commonly used to discriminate against the unwanted waves as well as background noise. Some data are also collected off the line, to permit the waves propagating out the plane of the section to be identified (Oliver, 1978)

With a perfect acquisition system, only small processing would be needed. This processing consist of application of a series of computer routines to the data acquired which is guided by the hand of the processing geophysicist. The interpreter is involved in all stages of processing to check that decisions do not badly alter the interpretability of the results in a negative manner. Processing can be done using one of the following methods listed below. (Rahman, _____ University of Rajshahi, Bangladesh).

1) Increasing resolution
2) Enhancing signal at the expense of noise
3) Providing velocity information
4) Collapsing diffractions and placing dipping events in their true subsurface location(i.e. Migration)

There are number of steps involved from seismic data acquisition to interpretation of subsurface structure. Some of the common steps are summarized below:

ACQUISITION	Static Correction
PROCESSING	Velocity Analysis
	NMO/DMO
	Stacking
	Migration(Time/Depth, Kirchhof's, f-k domain
INTERPRETATION	Seismic data to subsurface geology

Table.1 showing the steps of data acquisition and processing. Source (Rahman, _____ University of Rajshahi, Bangladesh).

3.4.1DATA ACQUISITION

The seismic profile data is normally in groups of seismic traces recorded from a common shot, known as shot gathers. The geophones may be distributed on either side of the shot, or only one side as shown in the figure below.

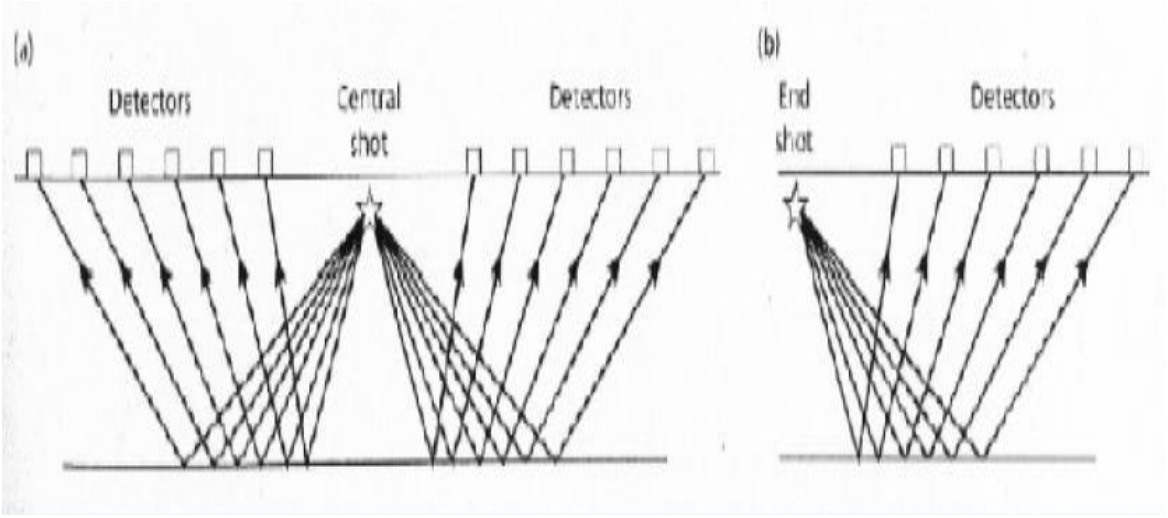

Fig.8. Shot-detector configurations used in multichannel seismic reflection profiling, (a) Split spread, or straddle spread, (b) Single-ended or on ended spread. Source (Hatton et al, 1986).

3.4.2 MULTIPLE SHOTPOINTS

This refers to reflections arising from the same point on the interface from more than one shot which is detected by different geophones. This common point of reflection is known as the common midpoint shown in the figure below.

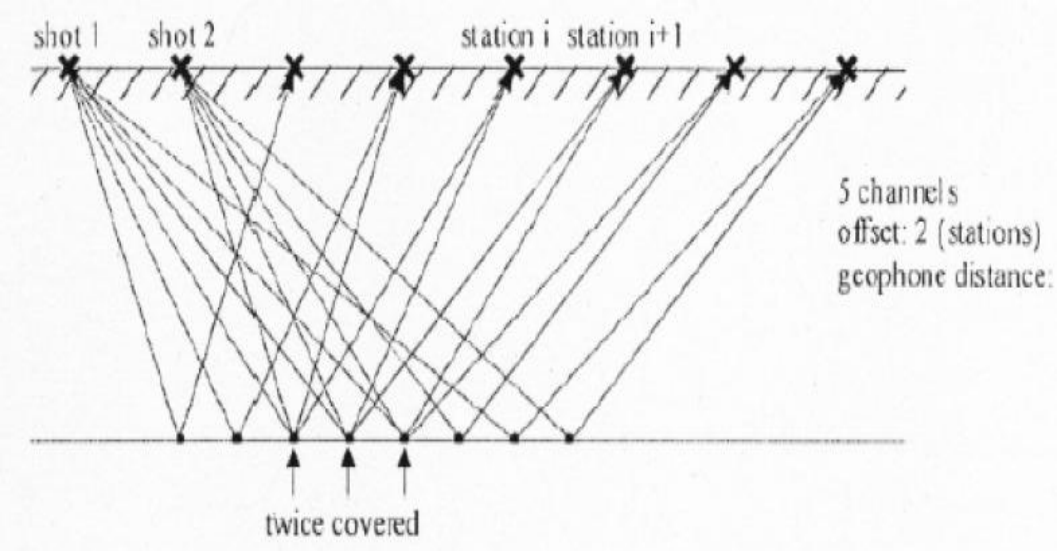

Fig.9. Data acquisition for reflection seismic. Source (Yilmaz, 1989).

The common midpoint (CMP) refers to the number of times the same point on a reflector is sampled as the fold of coverage. The CMP gather lies in the heart of seismic processing for two main reasons:

i) The variation of travel time with offset, the moveout will depend only on the velocity of the subsurface layers (horizontal uniform layers) and the subsurface velocity can be derived.

ii) The reflected seismic energy is usually very weak. It is imperative to increase the signal to noise ratio of most data.

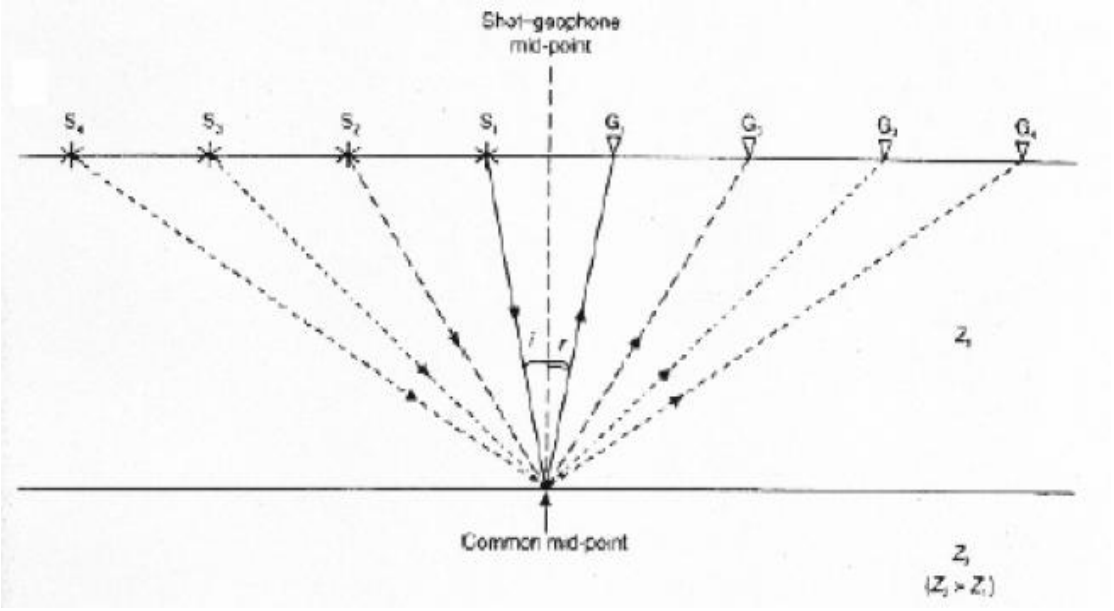

Figure. 10. Shows an example of the principle of the common midpoint over an interface. Source (Bracewell, 1983).

3.4.3 STATIC CORRECTION

This type of correction is applied to seismic data to compensate for the effects of variations in elevation, weathering thickness, weathering velocity, or reference to a datum. The purpose of this is to determine the reflection arrival times which would have been observed in all measurements. This is made on a flat plane with no weathering or low velocity material present. These corrections are based on uphole data, refraction first break or event smoothing.

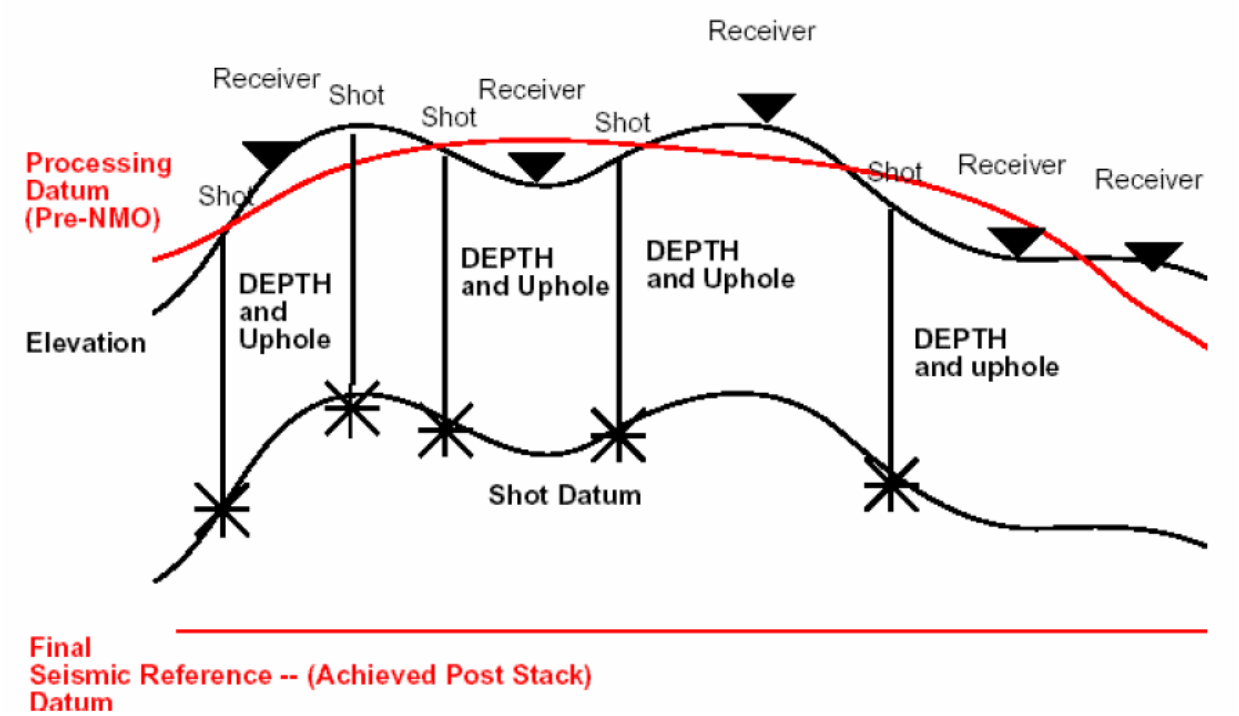

Fig.11. Showing the Datum Static Terminologies. Source (Rahman, _____ University of Rajshahi, Bangladesh).

3.4.4 STACKING (VELOCITY ANALYSIS, NMO/DMO)

This is an approach of iterative process of applying NMO, DMO and standard velocity analysis. DMO improves the quality of the stack and the usefulness of the stacking velocity field. A variety of methods are available (constant velocity stacks, constant velocity gathers, semblance) which work to different extents with different data types. NMO and DMO are used at the final velocity field after convergence.

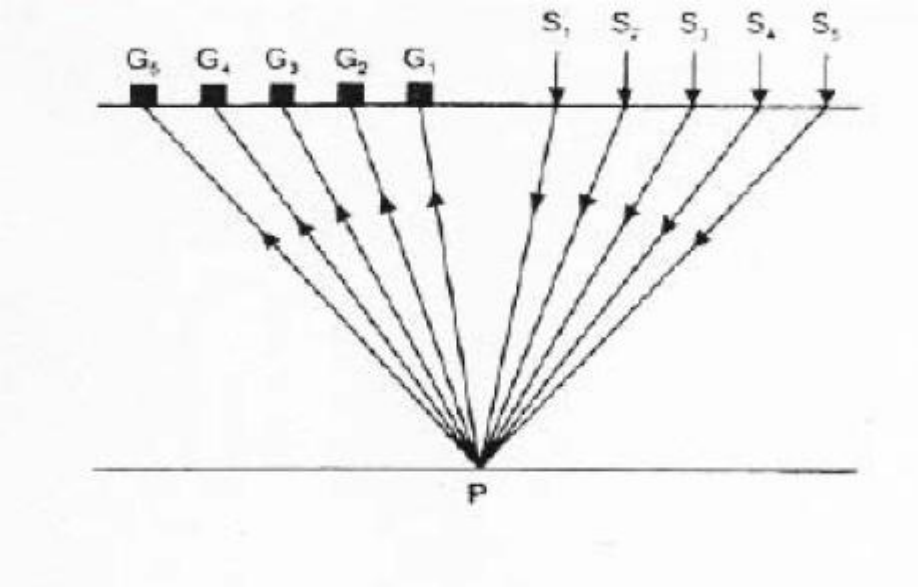

Fig 12. Shows source-receiver layout and corresponding ray paths for common point spread. Source (Bracewell, 1983).

The results of the seismic traces are also illustrated in the figure 13 below. This shows how the reflection events are aligned- and the final stacked traces.

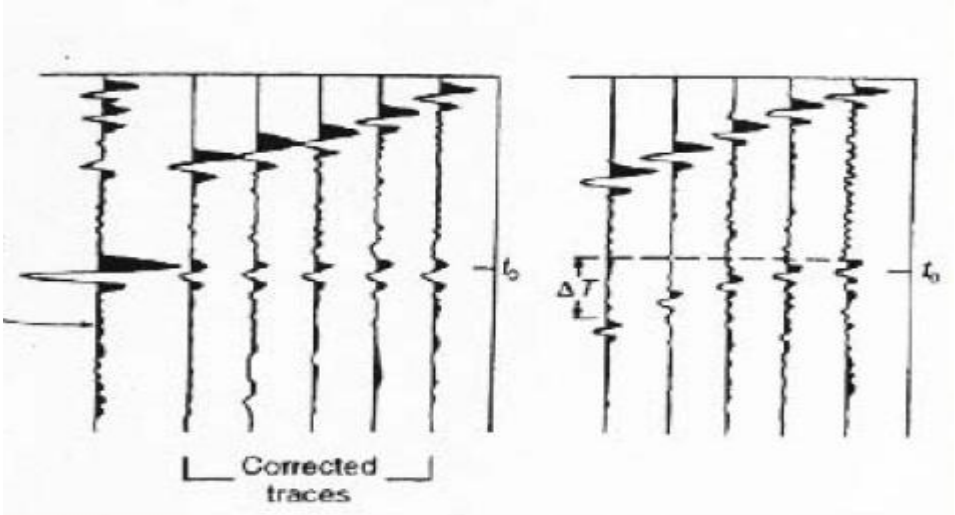

Fig. 13 shows both corrected (on the left) and uncorrected (on the right) traces. Source (Bracewell, 1983).

3.4.5 MIGRATION

Migration will result to the final product, either as depth or time. Migration can be applied using velocities based on our velocity analysis if they are good enough. This is done by testing a range of different velocities to determine which collapse diffraction correctly, or by using other information. Care is required to produce a generally smooth velocity field. A seismic section obtained before and after migration is shown below.

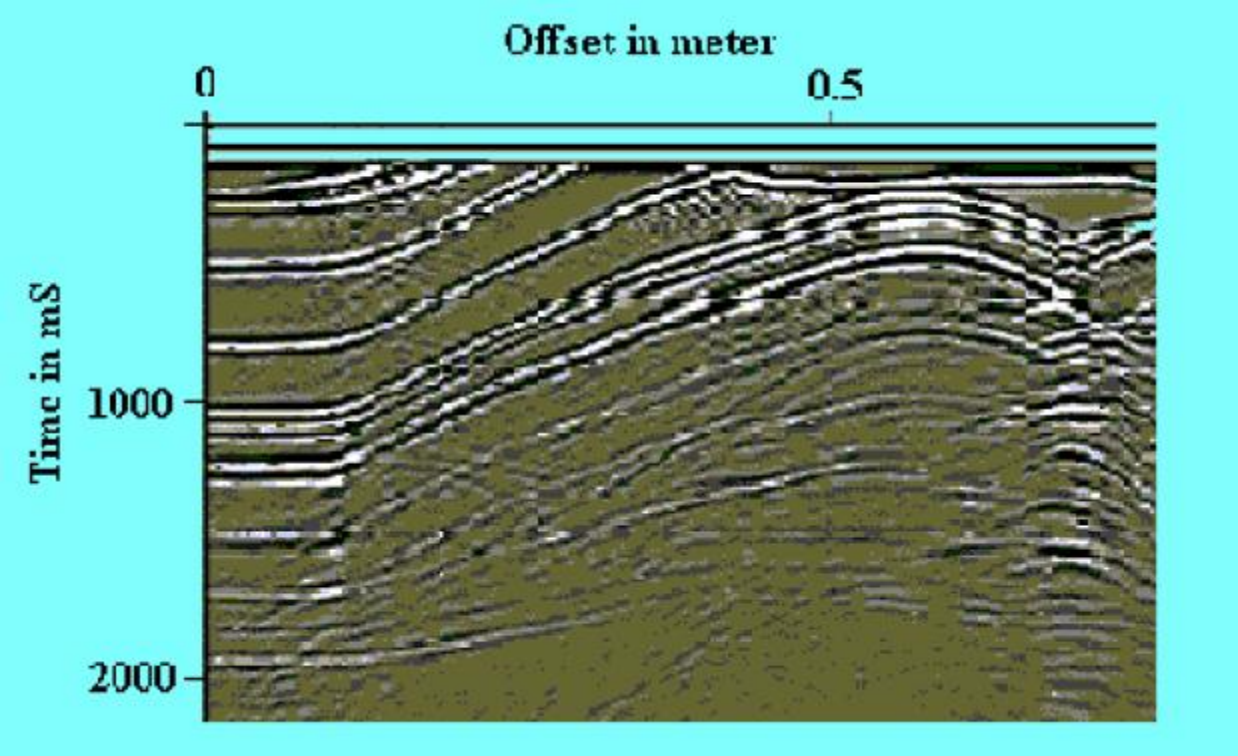

Fig. 14 shows a stacked section. Source (Rahman, _____ University of Rajshahi, Bangladesh)

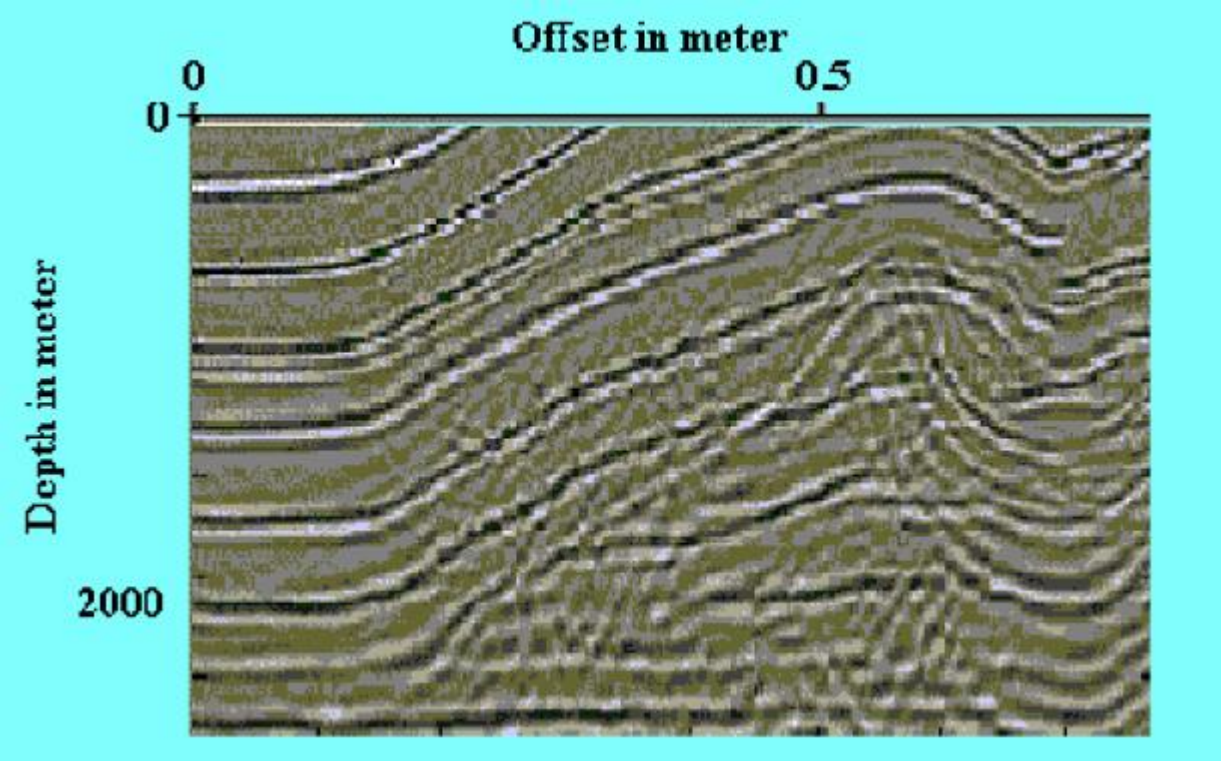

Fig. 15 shows the Post stacked migrated section. Source (Rahman, _____ University of Rajshahi, Bangladesh).

3.4.6 INTERPRETATION

Seismic stratigraphy is a technique for interpreting stratigraphic information from seismic data. The resolutions of the seismic reflection follow gross bedding and as such they approximate time lines. The key is that the contrast represented by seismic lines comes from bedding surface and not lateral variation (facies changes) as shown in the diagram below.

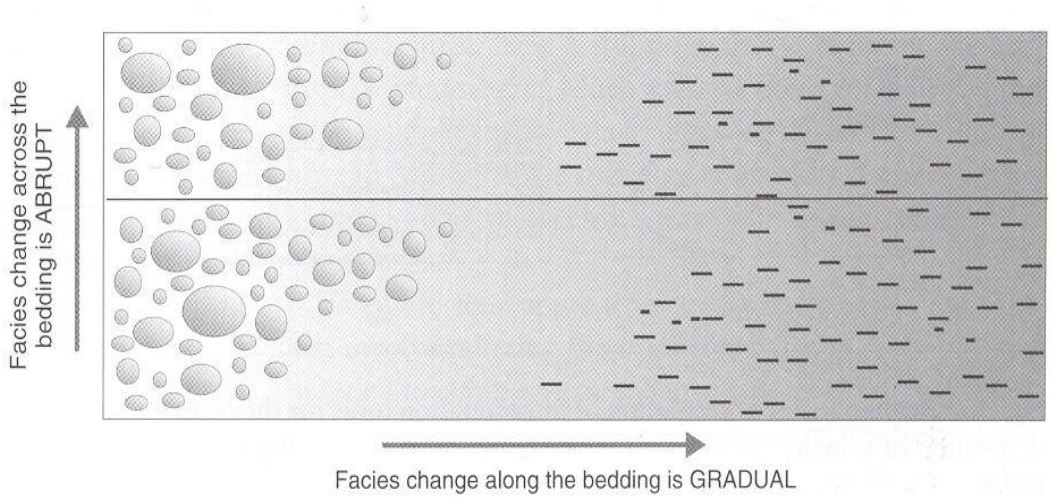

Fig.16 showing the facial changes from bedding changes.

Also understanding the resolution is also very important for seismic interpretation. For example vertical resolution can be defined as the minimum vertical distance between two interfaces needed to give rise to single reflection that can be observed on a seismic section. In a single noise free-seismic trace this is governed by the wavelength of the seismic signal. The shorter the wavelength (and hence higher the frequency) the greater the vertical resolution.

In addition to bed thickness constrains there are three other factors that limit final resolution of the seismic data.

1) The earth acts as a filter that progressively attenuates the high-frequency components of the seismic data
2) Acoustic velocity increases with depth due to compaction and increased cementation. This increases the wavelength of the signal with detrimental effect on the resolution.
3) If there is high ambient noise on the raw data, the processing stream may include a high-cut-filter.

In the interpretation of stratigraphy, the following steps are applied:

1) Determine the vertical and horizontal scale of the section. This is to find out the header or the seismic data if the section has been migrated, and whether it is marine or land data.
2) To divide the seismic data into discrete natural stratigraphic packages that makes up the section.
3) Identify and mark reflection terminations. It is a good idea to ignore zones of broken or chaotic reflections and to concentrate on better data. This can be interpreted later. Where reflection terminates in consistent manner they define a line on a seismic surface.

This is the final section of the seismic processing steps. Subsurface geologies are generally derived from this unit.

3.5 RESEARCH METHODOLOGY

1. This study involves the use of already processed synthetic data set in the interest of true amplitude recovery and AVO analysis.
2. A hypothetical gas-sand model is devised. This model consists of gas-sand layer encased in two shale layer as shown in the diagram below. This model is purposely simple, with the interface in question being shale over gas-sand using the velocities and densities (for gas-sand and shale) given in Castagna (1983).

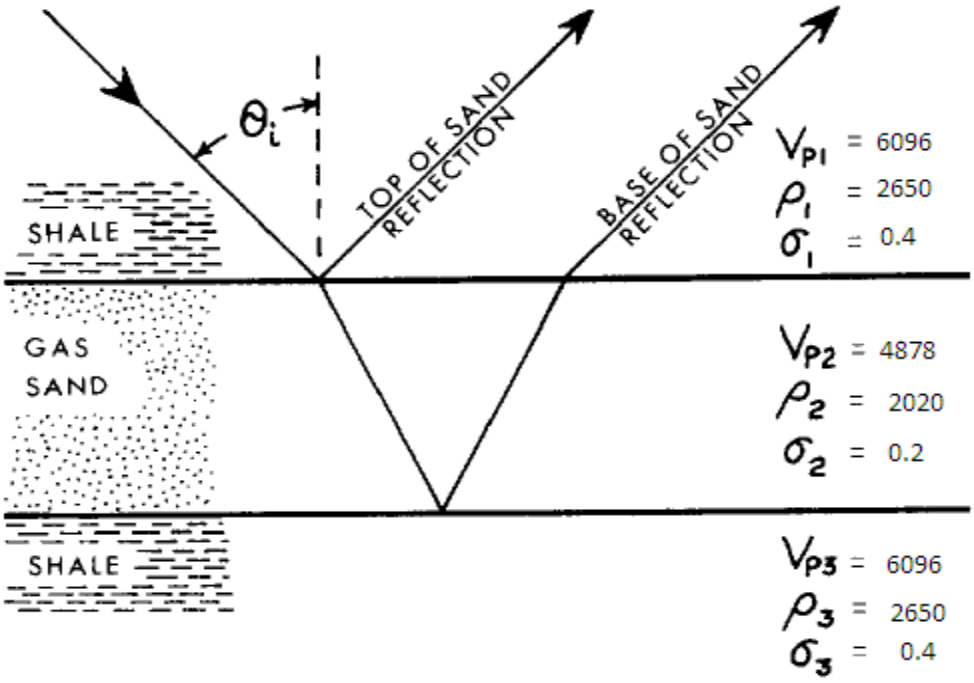

Fig. 17 Three layer hypothetical gas-sand model. Source (Ostrander, 1984).

3. The data consist of P and S wave velocities, densities and Poisson's ratio for different layers of Zoeppritz models (castagna, 1983). The synthetic data set consist of a number of offsets with different layers each recorded at different offsets giving a range of incident angles from 0 to 40 degrees. The synthetic data include the P-wave direct arrival, P-P reflection, P-SV reflection, and S-wave direct arrival. The data consist of P and S wave velocities, densities and Poisson's ratio for different layers of Zoeppritz models.

4. Using some published values(Castgna, 1993) of P-wave velocities, densities and Poisson's ratio of the two layers, the S-wave velocities for each of the layers was calculated from the formula shown below

$$V_s = \sqrt{\frac{2\sigma V_p^2 - V_p^2}{2\sigma - 2}} \qquad \text{..... (50)}$$

The formula above is derived from the Poisson's equation below

$$\sigma = \frac{1/2\left(V_p/V_s\right)^2 - 1}{\left(V_p/V_s\right)^2 - 1} \qquad \text{..... (51)}$$

5. **Matlab Implementation:** Calculation can be implemented in a Matlab by formulas to solve first snell's law, then the Zoeppritz equations by defining the Determinant and coefficient matrices for each incident angle from 0 to 90 degrees. These matrices are inverted and multiplied to calculate each of the resultant wave amplitudes for the incident angle using the formulas. Compressional and shear velocities for the layers above and below the interface as well as densities is used as input variables in the model.

6. This Matlab implementation is used Plot the reflection coefficient versus incident angle using the published and computed values for the layers. The values of the first layers are constant with changing values in the second layer.

7. The Plots of the P-wave reflection coefficient versus incident angle for models derived from the table below is used to analyze the reflection coefficients as a function of the angle of incidence for a simple three-layer, gas-sand model.

8. Based on Rutherford and Williams (1989) AVO reservoir classification, each of the plots was assigned to each of the class based on the amplitude of the reflection as a function of angle.

CHAPTER FOUR

RESULTS AND DISCUSSIONS

4.1 INTRODUCTION

This chapter seeks to throw more light on the Amplitude versus Offset using seismic data. This method of AVO analysis was tested by plotting the processed data amplitudes from Castagna (1993) and the theoretical reflection coefficients versus incident angle. The range of AVO effects for sandstone reservoirs is analyzed with the Zoeppritz P-wave reflection coefficient written in Matlab script. The model for the gas-sand reservoir is simple one consisting of a gas-filled sand encased in shale. Fig. 1 shown in chapter 3 is a schematic diagram that shows the top and base interface of the reservoir model. This script was also used to plot the reflection coefficient versus angle of incidence shown in the Figures below.

4.2. DATA ANALYSIS

To ensure that the information that will be used for the analysis is of high quality and deduce meaningful indications from the data. An already acquired and processed data was obtained from (Castagna, 1993), which was used in the AVO analysis based on the P-wave reflection against the incidence angle. In the assessment of the AVO plot, the following considerations were made.

1. The effect of change of the reflection coefficient with respect to angle of incidence.

2. The effect of the Poisson's ratio in AVO analysis.

3. The effect of P and S wave velocities on AVO analysis.

4. The effect of density on AVO analysis.

The tables below shows the various P-wave velocities [V_p (m/s)], S-wave velocities [V_s (m/s)], Densities[ρ (kg/m3)] and Poisson's ratios[σ] of different shale, gas-sand layers for different interface. The top (1st medium) is shale and the other models being gas-sand.

Layers	V_p(m/s)	V_s(m/s)	ρ (kg/m3)	Poisson's ratio σ
Top(1st medium)	6096	3258.5	2650	0.3
Model A	1829	977.6	795	0.3
Model B	2521	1347.5	1095	0.3
Model C	3048	1629.2	1325	0.3
Model D	4267	2280.8	1855	0.3
Model E	4877	2606.9	2120	0.3

Table. 2a. Parameters of some layers for five Zoeppritz models from Castagna (1993) for gas-sand structures. The parameter of the top layer is kept constant with a constant Poisson's ratio of 0.3 across the interface.

Layers	V_p(m/s)	V_s(m/s)	ρ (kg/m3)	Poisson's ratio σ
Top(1st medium)	6096	3733.0	2650	0.2
Model A	1829	1120.0	795	0.2
Model B	2521	1260.5	1095	0.2
Model C	3048	1866.5	1325	0.2
Model D	4267	2612.9	1855	0.2
Model E	4877	2986.5	2120	0.2

Table. 2b. Parameters of some layers for five Zoeppritz models from Castagna (1993) for gas-sand structures. The parameter of the top layer is kept constant with constant Poisson ratio of 0.2 across the interface.

Layers	V_p(m/s)	V_s(m/s)	ρ (kg/m3)	Poisson's ratio σ
Top(1st medium)	6096	2488.6	2650	0.4
Model F	4877	2987.2	2120	0.2
Model G	5444.2	3333.9	2360	0.2
Model H	6096	3733.3	2650	0.2
Model I	6775	4148.8	2950	0.2
Model J	7621.8	4667.8	3313	0.2

Table. 3a. Parameters of some layers for five Zoeppritz models from Castagna (1993) for gas-sand structures. The parameter of the top layer is kept constant with a reduction of Poisson's ratio across the interface from 0.4 to 0.2.

Layers	V_p(m/s)	V_s(m/s)	ρ (kg/m3)	Poisson's ratio σ
Top(1st medium)	6096	3258.4	2650	0.3
Model F	4877	2987.2	2120	0.2
Model G	5444.2	3333.9	2360	0.2
Model H	6096	3733.3	2650	0.2
Model I	6775	4148.8	2950	0.2
Model J	7621.8	4667.8	3313	0.2

Table. 3b. Parameters of some layers for five Zoeppritz models from Castagna (1993) for gas-sand structures. The parameter of the top layer is kept constant with a reduction of Poisson's ratio across the interface from 0.3 to 0.2.

Layers	V_p(m/s)	V_s(m/s)	ρ (kg/m3)	Poisson's ratio σ
Top(1st medium)	6096	3733.0	2650	0.2
Model K	1829	746.65	795	0.4
Model L	2521	1029.5	1095	0.4
Model M	3048	1244.3	1325	0.4
Model N	4267	1741.9	1855	0.4
Model O	4877	1219.2	2120	0.4

Table. 4a. Parameters of some layers for five Zoeppritz models from Castagna (1993) for gas-sand structures. The parameter of the top layer is kept constant with an increase of Poisson's ratio across the interface from 0.2 to 0.4.

Layers	V_p(m/s)	V_s(m/s)	ρ (kg/m3)	Poisson's ratio σ
Top(1st medium)	6096	3733.0	2650	0.2
Model K	1829	955	795	0.3
Model L	2521	1347.5	1095	0.3
Model M	3048	1629.2	1325	0.3
Model N	4267	2280.8	1855	0.3
Model O	4877	2120.0	2120	0.3

Table.4b. Parameters of some layers for five Zoeppritz models from Castagna (1993) for gas-sand structures.. The parameter of the top layer is kept constant with a reduction of Poisson's ratio across the interface from 0.2 to 0.3.

4.3 RESULTS

4.4 DIAGRAMS OF DIFFERENT AVO PLOTS

The results of the plots established the change in reflection coefficients with the incident angle which is dependent on Poisson's ratio difference across the interface.

4.4.1 FIGURES OF CONSTANT POISSON RATIOS.

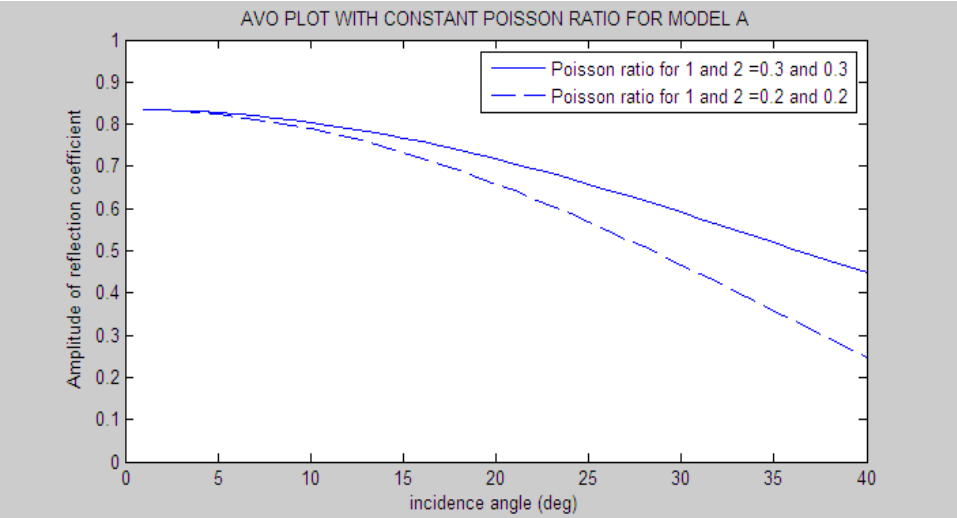

Fig 17a. P-wave reflection coefficient versus incident angle for model A given in Table 2a and 2b for constant Poisson ratio of 0.2 and 0.3 with varying values of the P-wave velocity contrast for each of the model across the interface.

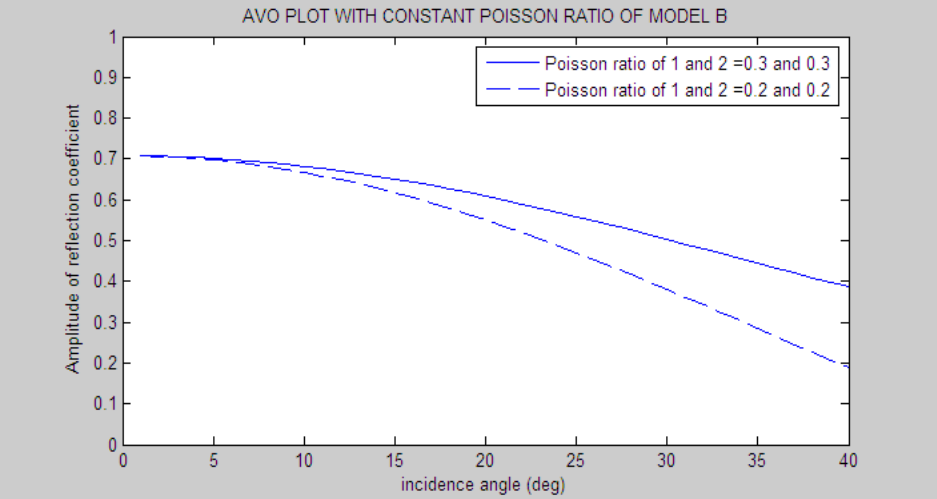

Fig 17b. P-wave reflection coefficient versus incident angle for model B given in Table 2a and 2b for constant Poisson ratio of 0.2 and 0.3 with varying values of the P-wave velocity contrast for each of the model across the interface.

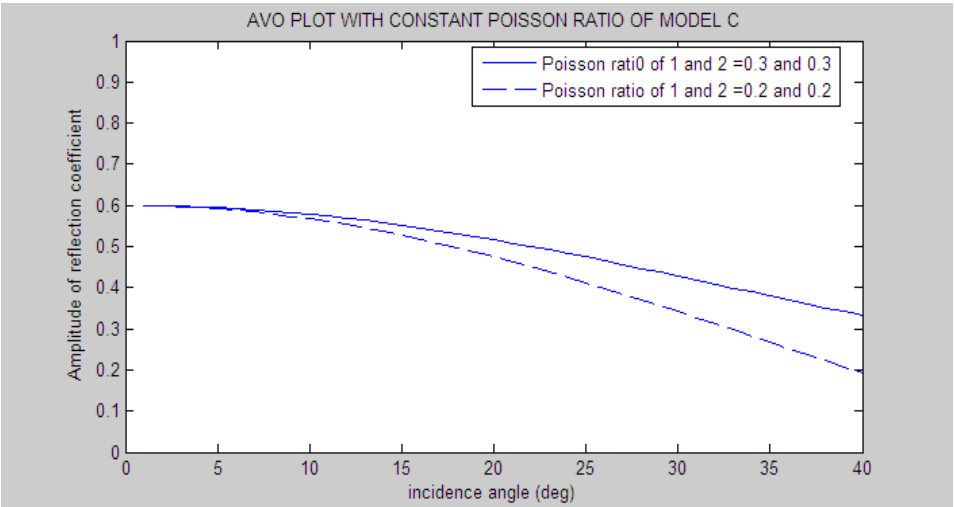

Fig. 17c. P-wave reflection coefficient versus incident angle for model C given in Table 2a and 2b for constant Poisson ratio of 0.2 and 0.3 with varying values of the P-wave velocity contrast for each of the model across the interface.

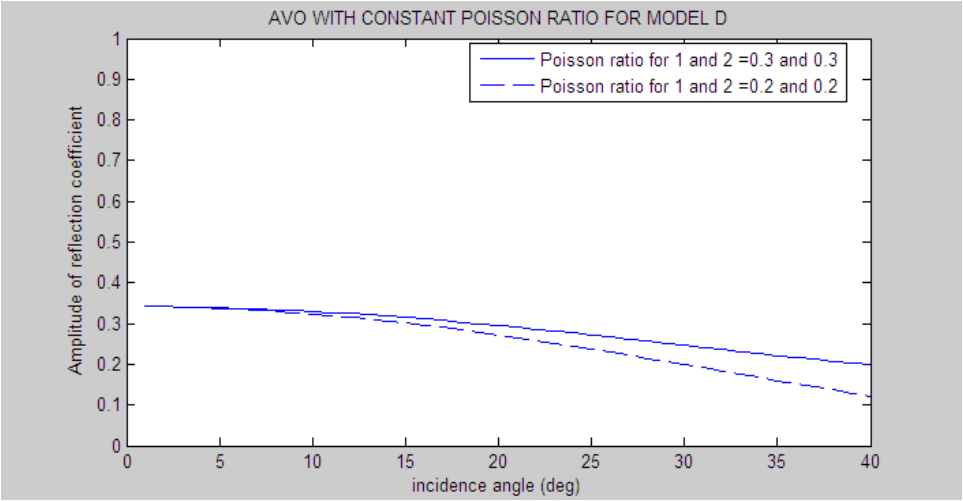

Fig 17d. P-wave reflection coefficient versus incident angle for model D given in Table 2a and 2b for constant Poisson ratio of 0.2 and 0.3 with varying values of the P-wave velocity contrast for each of the model across the interface.

4.4.2 FIGURES SHOWING REDUCTION IN POISSON RATIO ACROSS THE INTERFACE.

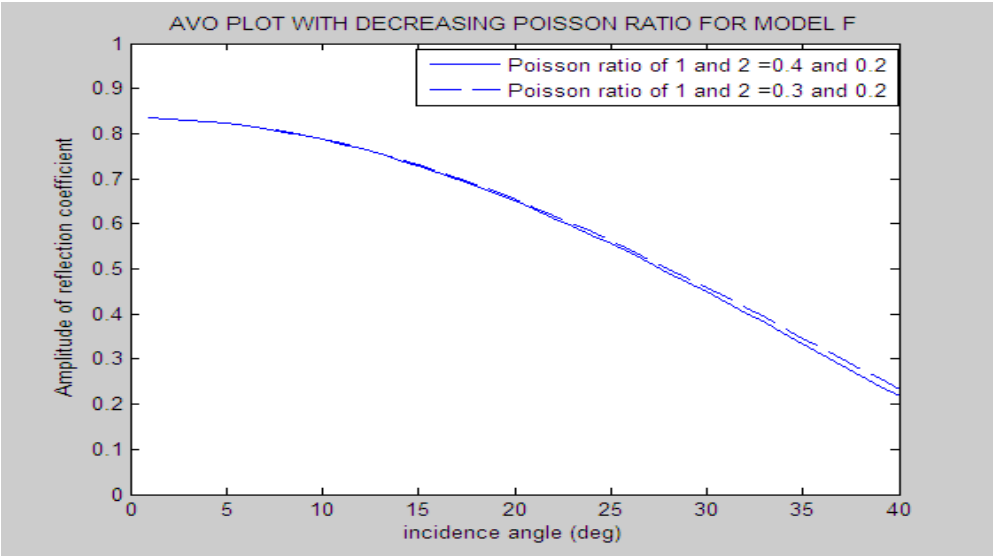

Fig 18a. P-wave reflection coefficient versus incident angle for model F given in Table 3a and 3b for decreasing Poisson ratio with varying values of the P-wave velocity contrast for each of the model across the interface.

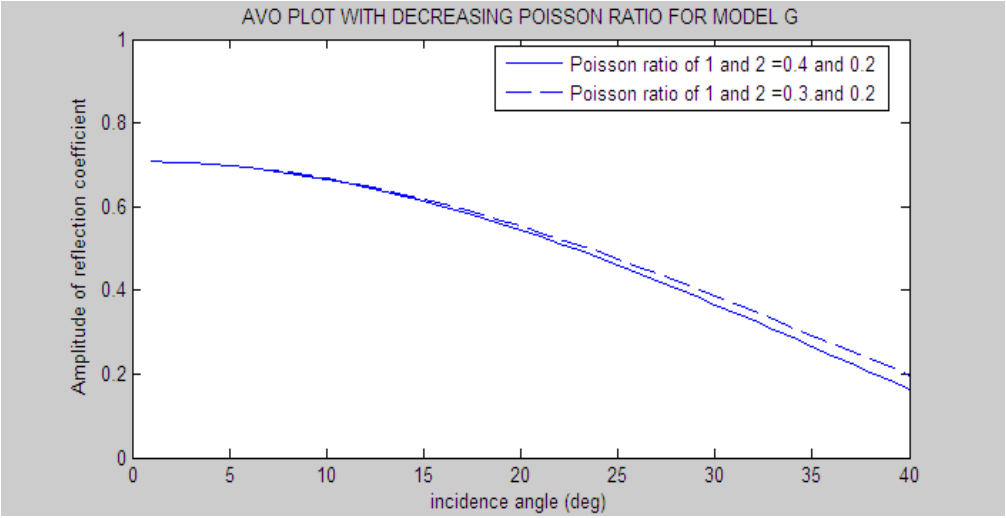

Fig 18b. P-wave reflection coefficient versus incident angle for model G given in Table 3a and 3b for decreasing Poisson ratio with varying values of the P-wave velocity contrast for each of the model across the interface.

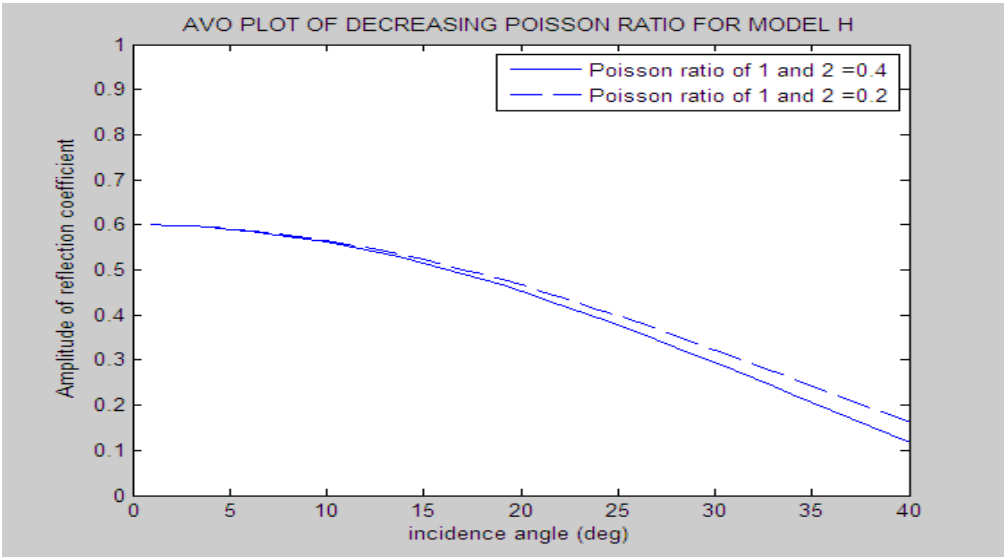

Fig 18c. P-wave reflection coefficient versus incident angle for model H given in Table 3a and 3b for decreasing Poisson ratio with varying values of the P-wave velocity contrast for each of the model across the interface.

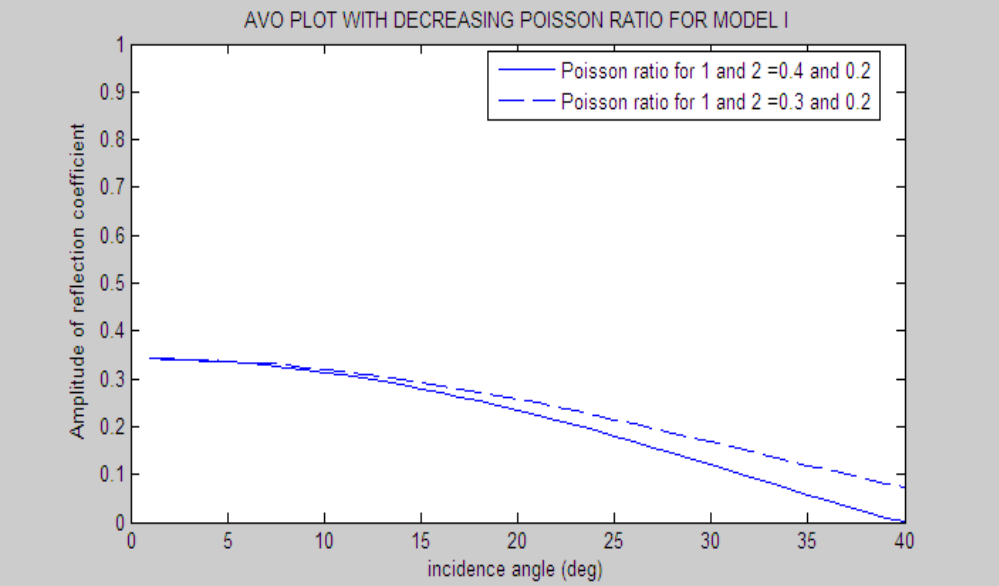

Fig 18d. P-wave reflection coefficient versus incident angle for model F given in Table 3a and 3b for decreasing Poisson ratio with varying values of the P-wave velocity contrast for each of the model across the interface.

4.4.3 FIGURES SHOWING INCREMENT IN POISSON RATIO ACROSS THE INTERFACE.

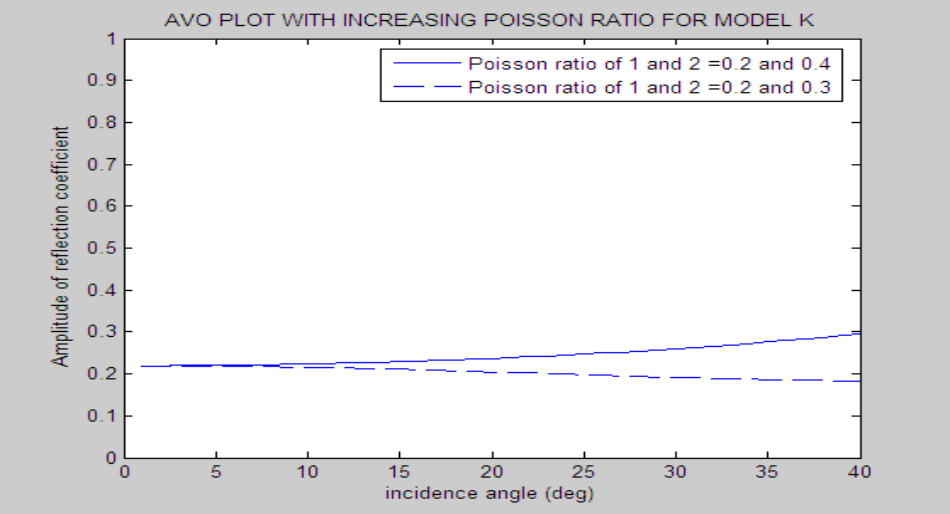

Fig 19a. P-wave reflection coefficient versus incident angle for model K given in Table 4a and 4b for increasing Poisson ratio with varying values of the P-wave velocity contrast for each of the model across the interface.

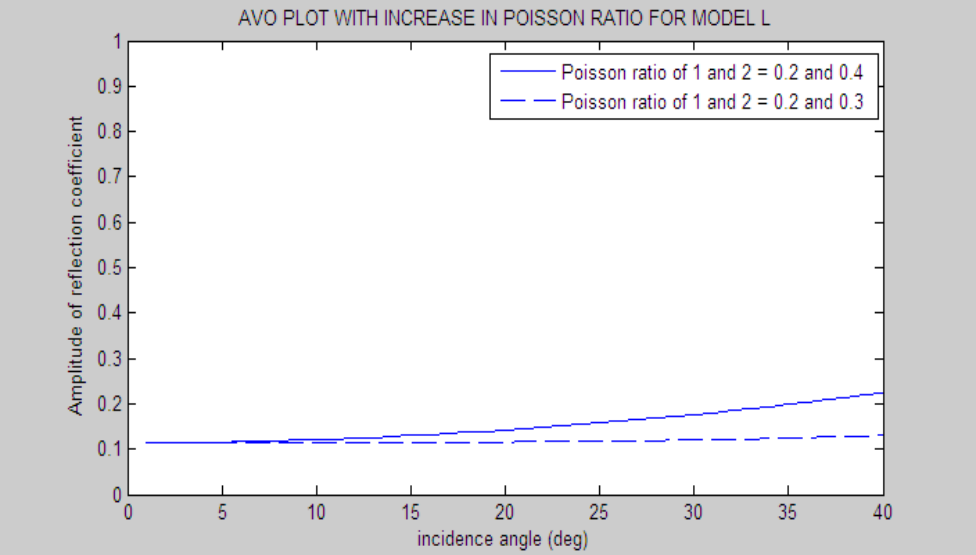

Fig 19b. P-wave reflection coefficient versus incident angle for model K given in Table 4a and 4b for increasing Poisson ratio with varying values of the P-wave velocity contrast for each of the model across the interface.

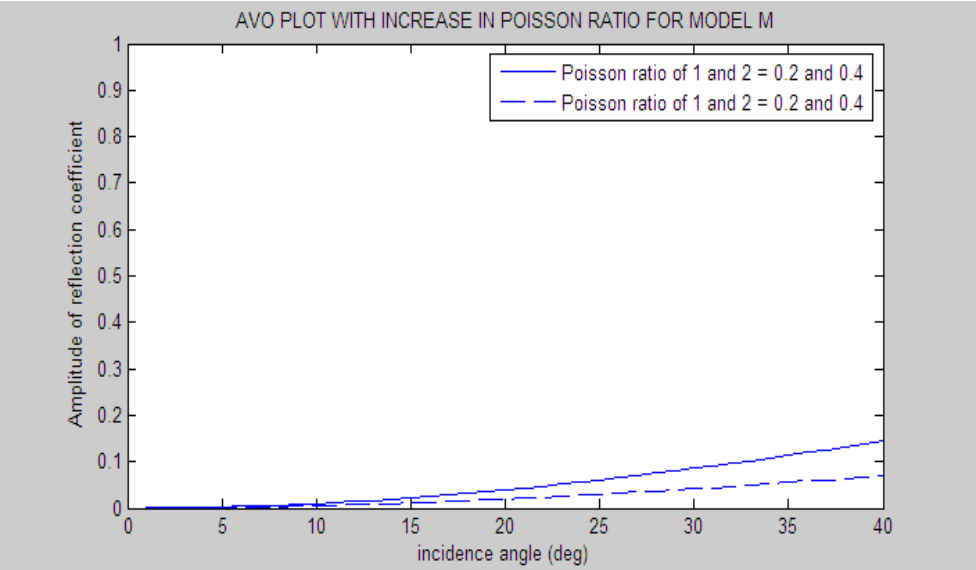

Fig 19c. P-wave reflection coefficient versus incident angle for model K given in Table 4a and 4b for increasing Poisson ratio with varying values of the P-wave velocity contrast for each of the model across the interface.

4.5 DISCUSSION OF RESULTS

According to the results of the Plots made using the simplified Zoeppritz equation. It can be deduced that an existing single reflecting/refracting interface between two isotropic media is dependent on the following variables.

1. Poisson's ratio in the upper medium.
2. Poisson's ratio in the lower medium.
3. P-wave velocity ratio between the two bounding media.
4. Density ratio between the two bounding media.

The parameters from the table 2a and 2b in chapter 3 was used in Plotting Fig. 17a, 17b, 17c and 17d, resulting in different normal-incidence reflection. The changes in plane-wave reflection coefficient as a function of angle of incidence for several instances are shown in the figures mentioned above. The solid curves are those reflection coefficients resulting from the gas-sand model shown in the methodology. The reflection coefficient changes from 0.83 to 0.46 from (17a), 0.71 to 0.40 for (17b), 0.60 to 0.33 for (17c) and 0.34 to 0.23 for (17d) over 40 degrees. Thus, the amplitude of seismic waveform resulting from this complex reflection increased approximately between the ranges of 35% and 45% over 40 degrees. The dash curves indicate what the reflection coefficient would be in the sand , showing constant Poisson's ratio of 0.2 and 0.3 of both media with varying velocities and densities. It can be deduce from the Plots that, the angle of incidence has only minor effects o P-wave reflection coefficients over propagation angle

which is commonly used in reflection seismology. Also in this case when the Poisson's ratio for both media is kept equal in as in the plots in Figures 1, the reflection coefficient at larger angle of incidence is thereby decreased. The velocity and density within the gas sand are substantially lower than encasing shale, giving rise to strong seismic reflections at the of the gas sand.

The parameters from the table 3a and 3b in chapter 3 was used in Plotting Fig. 18a, 18b, 18c and 18d, resulting also in different normal-incidence reflection. This Figures show P-wave reflection coefficient from an interface, with the incident medium having a higher Poisson's ratio than the underlying medium. The solid curve represents a contrast in Poisson's ratio of 0.4 to 0.2, while the dashed curve represents a contrast of 0.3 to 0.2. It can therefore be concluded from the Plots that if Poisson's ratio decreases going to the underlying medium, the reflection coefficient decreases algebraically with increasing angle of incidence. This means positive reflection coefficient may reverse polarity, while negative reflection coefficients increase in magnitude (absolute value) with increasing angle of incidence. As Poisson's ratio decrease in the second medium (as would occur when gas replaces brine), the reflection coefficient becomes more negative with increasing offset. This is contrast to the usual abused rule of thumb that "gas causes amplitude to increase with offset/angle" which is only correct for near zero or negative $R_{p.}$ Thus increased amplitude results from increasing the magnitude of the reflection coefficient in both positive and negative direction. These Figures also show the effect of lowering the Poisson's ratio in the second medium for all V_{p2}/V_{p1} ratios.

The parameters from the table 4a and 4b in chapter 3 was used in Plotting Fig. 19a, 19b, and 19d, resulting also in different normal-incidence reflection. These Plots is the direct opposite case to that illustrated in Figures 2 above. In this instance, the Poisson's ratio increase going from the

incident medium to the underlying medium. In this situation, the reflection coefficients increase algebraically with increasing angle of incidence. Negative reflection coefficients may also increase polarity, and positive reflection coefficients increase in magnitude with increasing angle of incidence. Thus an increase in Poisson's ratio for the underlying medium causes an increase of the reflection coefficient at large angle of incidence. When in this case the Poisson's ratio for the incident medium is increased, the reflection coefficient at larger angles of incidence is thereby decreased.

4.6 CLASSIFICATION OF THE AVO PLOTS

The Figures Plotted above show a set of reflection coefficient AVO curves for some interface calculated for range of normal incidence reflection coefficient R_o. The curves in the Figures have a range of Poisson's ratio between 0.40 and 0.20 and densities ranging between 3.50 and 0.795 g/cm^3.

The AVO curves of Fig. 17a, 17b, 17c, 18a, 18b and 18c can be assigned to class I of the AVO class. This is because all these curves have a positive reflection coefficient curve at zero offset/angle (high impedance) and they decreases in magnitude with offset/angle. This magnitude of the rate of change of amplitude with offset/angle (referred to as "gradient") for the class I sand is usually greater than the other class. The gradient depends on the R_o as well as the Poisson ratio contrast across the interface. In general the gradient decreases as R_o decreases for a decrease in Poisson's ratio for all these curves belonging to class I sands. The magnitude of reflectivity of these AVO curves assigned to class I initially decrease with offset/angle and changed polarity at adequate offset/angle availability. Since these curves have high amplitude at zero offset/angle, large fractional change in amplitude is possible when the far trace reflectivity is near zero. This

characteristic of AVO curves is normally for acoustically hard rock, where at normal incidence and smaller incident angles, the amplitude decreases with angle of incidence or offset in the amplitude-versus-offset/angle domain.

The AVO curves of Fig. 17d and 18d can be assigned to class II of the AVO class. These curves have the same impedance as the encasing material. The zero-offset/angle reflection coefficients for this curves assigned to the AVO class II are close to zero, with large fractional changes in reflectivity occurring from near to far offset/angle. This helps to enhance the delectability of the sands. The gradient of these curves are large in magnitude but are generally less than those for class I sands. The small offset/angle reflectivity of these curves of class II sands is close to zero and is detectable in the presence of noise. Their polarity changes if R_o is positive, but it usually not detectable, because it occurs at a near offset where the signal is below the noise level.

CHAPTER FIVE

CONCLUSIONS AND RECOMMENDATIONS

5.1 CONCLUSIONS.

AVO processing is an important tool for the interpretation of subsurface rock properties. In this study we have produced AVO curves using the Zoeppritz analytical equation for the interface between different media, and we have explored the dependence of amplitude reflections from Poisson ratio and gas content.

In light of the results and discussions, it can be concluded that;

1. Poisson's ratio has a strong influence on changes in reflection coefficient as a function of incidence angle.
2. Analysis of seismic reflection amplitude versus shot-to-group offset can in many cases distinguish between gas-related amplitude anomalies and other type of amplitude anomalies
3. Analysis and classification of AVO effects is absolutely dependent on careful seismic processing.
4. AVO analysis is one technique for getting information to answer questions on lithology, porosity and fluid content.
5. AVO technique gives a robust and inexpensive method for identifying potential reservoirs and it is also a technique that adds dimension to studies done only with stacked seismic data.
6. Amplitude variations with offset/angle seen on seismic data are due to contrasts in elastic rock properties.
7. The change in lithology, porosity and fluid affects Plots in AVO space.

5.2 RECOMMENDATION

The method of analysis presented here has proven to be useful in many of the world's gas provinces. However, the methods are not fool proof and experience has shown them to fail on occasion.

Other factors which affect observed reflection amplitudes versus offset need to be considered. Thus amplitude balancing during processing is quite important.

Additional information on Poisson's ratios for other rock types needs attention as well as the effects of depth of burial and sediment consolidation on Poisson's ratio.

REFERENCES

Muskat M and Meres MW 1940: "Reflection and Transmission Coefficients for Plane Waves in Elastic Media." Geophysics 5: 115-148.

Amplitude-versus-offset analysis using the vertical seismic profile. Craig A. Coulombe, Robert R. Stewart and Michael J. Jones 1990, p.464.

Koefoed O: 1995"On the Effect of Poisson's Ratios of Rock Strata on the Reflection Coefficients of Plane Waves. "Geophysical Prospecting 3 (December 1955): 3-38-381-387.

Koefoed 1962, Reflection and transmission coefficients for plane longitudinal incident waves:Geophys. Prosp., 10, 304-351.

Ostrander, W. J., 1984, Plane-wave reflection coefficients for gas sands at non-normal angles of incidence: Geeophysics, vol. 49, No. 10, 1637-1648

Aki, K and Richards, P.G., 1980: Quantitative Seismology. Theory and Methods Vol 1. San Francisco, California, USA: WH Freeman and Co.: 123-155.

Coulombe, C. A. et al 1993. Amplitude-versus-offset analysis using the vertical seismic profile.

Rutherford, S.R., and Williams, R.H., 1989, Amplitude-versus-offset variations in gas sands: Geophysics. v. 54, p. 680-688.

Chiburis, E., Leaney, S., Skidmore, C., Franck, C., and McHugo, S., 1993. Hydrocarbon Detection with AVO. Page 1-3.

Xu and Bancroft, J. C., 1997. Joint AVO analysis of PP and PS seismic data. CREWE research report vol. 9

Castagna, J. P., and Smith, S.W., 1994. Comparison of AVO indicators: A modeling study: Geophysics, 59, no. 12, 1849-1855.

Smith, G.C., and Sutherland, R.A., 1996. The fluid factor as an AVO indicator: Geophysics, 61, no. 5, 1425-1428.

Green, G., 1839. On the Laws of Reflection and Refraction of Light, in Transactions of the Cambridge Philosophical Society 7: 245. Reprinted in Mathematical Papers of the Late George Green. London, England: Macmillan, 1871.

Macelwane, J.B and Sohon, F.W., 1936. Introduction to theoretical Seismology. New York, USA: John Willey & Sons, Inc.: 147-179.

Shuey, R.T., 1985. A simplification of the Zoeppritz equations: Geophysics, 50, no. 4, 609-614

Sheriff, R., 1995. Exploration Seismology: Cambridge.

Castagna, J. P., 1995. Applied AVO Analysis: Use and Abuse of Amplitude variation with Offset (1995 Fall SEG Distinguished Lecture).

Castagna, J. P., and M. Backus, 1993, Offset dependent reflectivity – Theory and practice of AVO analysis: Investigation in geophysics, 8.p.3

Zhang, H and Brown, R. J., 2001, A Review of AVO analysis: CREWES Research Report, Vol 13.p.358

Bortfeld, R., 1961. Approximation to the Reflection and Transmission coefficients of Plane Longitudinal and Transverse waves. Geophysical Prospecting 9: 485-502.

Smith, G.C. et al., 1987. Weighted stacking for rock property estimation and detection of gas: Geophysical Prospecting, 35, no. 9, 993-1014.

Tooley, R. D., Spencer, T. W., and Sagoci, H, F., 1965. Reflection and transmission of plane compressional waves: Geophysics, 30, 552-570.

Muskat, M., and Meres, M. W., 1940, Reflection and transmission coefficients for plane waves in elastic media: Geophysics, 5, 149-155.

Wardhana, R. A., 2001. Analysis of Time-Lapse Seismic Technology Using a Physical Model of Porous Channel Sand: University of Houston, Faculty of Geoscience.

Zhang, T., 2008. A general constitutive relation for linear elastic foams. Int. J. Mech. Sci. 50(6), 1123-1132.

Biot, M.A., 1956. “Theory of propagation of elastic waves in a fluid saturated porous solid” I. Low frequency range and II. Higher- frequency range. J. Acoust. Soc. Am., 28, 168-191.

Gassmann, F., 1951. “Über Die Elastizität poröser Medien” Vier. der Natur. Gesellschaft in Zürich, 96 1-23.

Kumar, D., 2006. A tutorial on Gassmann Fluid substitution: Formulation, Algorithm & Matlab code: Chevron Energy technology company, California.

Mavko, G., Mukerji, T., Dvorkin, J., 1998. “The Rock Physics Handbook” Cambridge University Press.

Brian J. Evans, 1997 A Handbook for Seismic Data Acquisition in Exploration,p.1-3

McGregor, 2007, Abrief Review of AVO Anomaly Classification, Geohorizons January 2007/34

Khattri, K., Mithal, R., and Gaur, V., 1979. Pattern space of seismic profiling applied to sediment logy: Geophysics, V. 53, p. 1276-1283.

Begay, D. K., Miller, R. D., Watney, W. L., and Xia, J. 2000. High-resolution P-and S-wave reflection to detect a shallow gas sand in southeast Kansas.

Barker, R. and D. Lapucha (1994), "Performance Comparison of Two Methods of Multiple Reference Station DGPS". Proceedings of The Institute of Navigation 7th International Technical Meeting, ION GPS-94, Salt Lake City, Utah, Sep 20-23, 1994, pp. 1035-

Oliver, J.E. "Exploration of the Continental Basement by Seismic Reflection Profiling." Nature 275 (1978): P.485-488.

Rahman, S. M.,……. Seismic Data Processing and Interpretation. Department of Applied Physics and Electronic Engineering. : University of Rajshahi, Bangladesh.

Yilmaz, O., 1989. Seismic Data Processing. Society of Exploration Geophysicists, USA.

Hatton, L., Worthington, M.H. and Makin, J., 1986. Seismic Data Processing Theory and Practice. Blackwell Scientific Publications, ISBN 0-632-01374-5.

Bracewell, R. N., 1983. The Fourier Transform and its Applications. McGraw-Hill, New York.

Castagna, J. P., 1983, Prediction of Fe-Mg site occupancies in pigeonite: Geophysical Research Letters, 10, 137-139

APPENDIX A

THE AKI-RICHARDS (1980) MATRIX REPRESENTATION OF THE KNOTT-ZOEPPRITZ EQUATIONS (FROM CASTAGNA AND BACKUS, 1993).

APPENDIX A-MATRIX REPRESENTATION OF THE KNOTT-ZOEPPRITZ EQUATIONS

In 1980, Aki and Richards give the Knott-Zoeppritz equations in a convenient matrix form. This type of matrix is well illustrated here.

For an interface between two infinite elastic half-spaces, there are sixteen reflection and transmission coefficients (see Figure A-1). In the Aki and Richards's notation, the coefficients are represented by two letters (e.g. ***PS***). The first letter indicates the type of incident wave and the second letter represents the type of derived wave. The acute (´) indicates an up going wave while a down going wave has a grave accent (`). Thus, ***PS*** is the down going P-wave to up going S-wave coefficient. With this notation, the scattering matrix is

$$Q = \begin{pmatrix} \grave{p}p' & \grave{s}p' & p'p' & s'p' \\ \grave{p}s' & \grave{s}s' & p's' & s's' \\ \grave{p}\acute{p} & \grave{s}\acute{p} & p\acute{p} & s\acute{p} \\ \grave{p}\acute{s} & \grave{s}\acute{s} & p'\acute{s} & s'\acute{s} \end{pmatrix} = \boldsymbol{P}^{-1}\boldsymbol{R}$$

Where **P** is the matrix

$$\begin{pmatrix} -\sin\theta_1 & -\cos\phi_1 & \sin\theta_2 & \cos\phi_2 \\ \cos\theta_1 & -\sin\phi_1 & \cos\theta_2 & -\sin\phi_2 \\ 2_{p1}V_{s1}\sin\phi_1\cos\theta_1 & {}_{p1}V_{s1}(1-2\sin^2\phi_1) & 2_{p2}V_{s2}\sin\phi_2\cos\theta_2 & {}_{p2}V_{s2}(1-2\sin^2\phi_2) \\ {}_{-p1}V_{p1}(1-2\sin^2\phi_1) & {}_{p1}V_{s1}\sin 2\phi_1 & {}_{p2}V_{p2}(1-2\sin^2\phi_2) & {}_{-p2}V_{s2}\sin 2\phi_2 \end{pmatrix}$$

And **R** is the matrix

$$\begin{pmatrix} \sin\theta_1 & \cos\phi_1 & \sin\theta_2 & \cos\phi_2 \\ \cos\theta_1 & -\sin\phi_1 & \cos\theta_2 & -\sin\phi_2 \\ 2_{p1}V_{s1}\sin\phi_1\cos\theta_1 & {}_{p1}V_{s1}(1-2\sin^2\phi_1) & 2_{p2}V_{s2}\sin\phi_2\cos\theta_2 & {}_{p2}V_{s2}(1-2\sin^2\phi_2) \\ {}_{-p1}V_{p1}(1-2\sin^2\phi_1) & -_{p1}V_{s1}\sin 2\phi_1 & -_{p2}V_{p2}(1-2\sin^2\phi_2) & {}_{p2}V_{s2}\sin 2\phi_2 \end{pmatrix}$$

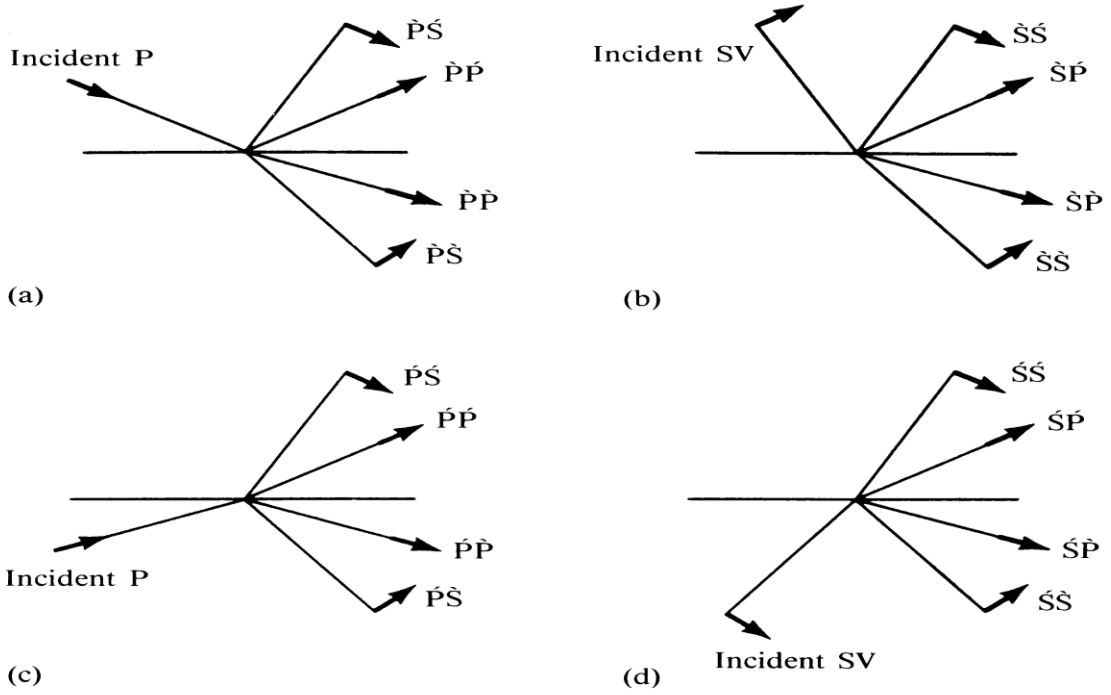

Notation for the sixteen possible reflection/transmission coefficients for P-SV waves at an interface between two different solid half-spaces. Short arrows show the direction of particle motion (from Aki and Richards, 1980).

EXCEPT OF THE MATLAB SCRIPT THAT WAS USED FOR THE AVO PLOT

```
clear all
close all
```

```
clc;
p1=6096;   % m/s p wave velocity firts layer
s1=3733;    % m/s
ro1=2650;  % kg/m^3

p2=1829;   % m/s p wave velocity second layer
s2=746.6;    % m/s
ro2=795;  % kg/m^3

cf=1;

for k=1:40

   teta(k)=k/180*pi;
   u=sin(teta(k))/p1;
   [dr,dt,ur,ut]=scatt(p1,p2,s1,s2,ro1,ro2,u,cf);
   Rpp(k)=dr(1,1);
end
plot(teta/pi*180,abs(Rpp))
xlabel('incidence angle (deg)')
ylabel('Amplitude of reflection coefficient')
axis([0 40 0 1])
```